View metadata, citation and similar papers at core.ac.uk

brought to you by CORE

provided by The University of Utah: J. Willard Marriott Digital Library

AN EXAMINATION OF DISLOCATIONS IN P-TYPE GERMANIUM WAFERS GROWN OFF AXIS BY ETCH PIT TECHNIQUE

by

Jason Lee Neff

A thesis submitted to the faculty of
The University of Utah
in partial fulfillment of the requirements for the degree of

Master of Science

Department of Metallurgical Engineering

The University of Utah

August 2014

Copyright © Jason Lee Neff 2014

All Rights Reserved

The University of Utah Graduate School

STATEMENT OF THESIS APPROVAL

The thesis of Jason Lee Neff

has been approved by the following supervisory committee members:

Sivaraman Guruswamy	, Chair	**4/14/2014** Date Approved
Michael L. Free	, Member	**4/14/2014** Date Approved
Zhigang Zak Fang	, Member	**4/14/2014** Date Approved

and by Manoranjan Misra , Chair of

the Department of Metallurgical Engineering

and by David B. Kieda, Dean of The Graduate School.

ABSTRACT

In recent years the demand for germanium has swiftly increased due to its use in Infrared (IR) optics, gamma-radiation detectors, and in large part to the importance as a substrate for concentrator multijunction celestial and terrestrial based solar cells. Because of the high cost of germanium, and the weight limits of space systems, germanium wafers used in multijunction space solar cells are ultra thin and therefore susceptible to failure due to defects laid in from Czochralski (CZ) crystal growth, and wafer processing. These defects can greatly alter or hinder the electrical properties of the device made from these germanium wafers because of stress, or affect the growth of any material such as gallium arsenide grown epitaxially on the germanium wafer. The ability to locate and measure these defects is critical in developing a growth and wafering process to produce dislocation free germanium crystals and ultrathin wafers cut from them.

A chemical etching solution has been found to reveal pits that correspond to dislocations in p-type germanium wafers. The etching solutions, which includes $Cu(NO_3)_2$ dissolved in HF & HNO_3 and H_2O_2 & HNO_3, are shown to disclose defect points for germanium wafers that were grown off the [100] plane 4°-8° towards the [111] plane to provide multiple and random lattice sites for high quality epitaxial growth. Alterations of the etch solution were also examined in order to develop a chemical polishing technique, which aided the turnaround time of dislocation examination. The morphology of the etched surface was examined with varying etch times. The surface of

the etched wafers was observed using a light microscope that possessed Nomarski Differential Interference Contrast (DIC) imaging capability.

For Haley, Conner, Leah and Jonah

TABLE OF CONTENTS

ABSTRACT.. iii

LIST OF FIGURES.. viii

LIST OF TABLES.. x

ACKNOWLEDGEMENTS.. xi

Chapters

1. INTRODUCTION 1

2. SCIENTIFIC BACKGROUND 8

2.1 Czochralski Crystal Growth 8
2.1.1 Segregation in Crystal Growth 12
2.1.2 Thermal Stresses in Crystal Growth 22
2.2 Germanium Wafer Processing 27
2.3 Dislocation Etch Pits 31
2.3.1 Chemical Dislocation Etch Solution 33

3. EXPERIMENTAL PROCEDURES 35

3.1 Sample Preparation 35
3.2 Etching Solutions 37
3.2.1 Solution Discovery 37
3.2.2 Etch Process 41
3.3 Evaluation of Dislocations and Density 42
3.4 Single Crystal Orientation 42

4. RESULTS AND DISCUSSION 43

4.1 Etch Pit Results 43
4.2 Etching Rates and Times 45
4.3 Alternative Polishing and Etching Processes 59

5. CONCLUSIONS 61

APPENDIX: VISUAL SCORE TABLE 63

REFERENCES 64

LIST OF FIGURES

1.1. Energy band structure of germanium....4

2.1. A sketch of the growth assembly for CZ crystal growth. 9

2.2 An image of a germanium crystal grown by CZ process....11

2.3 A sketch of the (a) 100 (b) 110 and (c) 111 crystal planes in germanium single crystal 13

2.4 A view of the (a) 100 (b) 110 and (c) 111 atomic lattices in germanium single crystal. 14

2.5 Two distinctly different solvent-rich phase diagram regions that illustrate (a) segregation coefficient k<1 and (b) segregation coefficient k>1 16

2.6 Variation of effective Ge segregation coefficient as a function of growth rate. The segregation coefficient for gallium in germanium is included for comparison 17

2.7 Schematic curve showing the impurity distribution across the solid-liquid interface for $k_o < 1$ 20

2.8 Schematic curves showing the temperature distribution across the solid-liquid interface for $k_o < 1$; (a) melt temperature; (b) actual thermodynamic equilibrium liquidus temperature....21

2.9 A schematic diagram illustrating the radial and axial temperature gradients in a single crystal being pulled from the melt....23

2.10 Optical micrograph of a preferentially etched germanium wafer revealing low angle boundary dislocations....25

2.11 Optical micrograph of a preferentially etched germanium wafer revealing low angle boundary dislocations and cellular structures 26

2.12 Flow chart for the germanium wafer production process 28

2.13 Subsurface damage of a wafer after slicing. 30

2.14 Etch pits in LiF single crystal 32

3.1 An image of a polished germanium wafer 38

3.2 Wafer surface after etching with Superexol for 75 seconds 40

4.1 Etch pits on a germanium wafer 44

4.2 Etch rate of of $CuNO_3$ (10%) : HNO_3 : HF (1:1:2) solution on germanium wafer 49

4.3 Etch rate of of $CuNO_3$ (10%) : HNO_3 : HF (1:1:2) solution on germanium wafers as a function of etch temperature. 50

4.4 Removal of material at each etching time tested. 53

4.5 Image of germanium wafer surface after 5 seconds of etching using $CuNO_3$ (10%) : HNO_3 : HF (1:1:2) solution. 54

4.6 Image of germanium wafer surface after 15 seconds of etching using $CuNO_3$ (10%) : HNO_3 : HF (1:1:2) solution. 55

4.7 Image of germanium wafer surface after 25 seconds of etching using $CuNO_3$ (10%) : HNO_3 : HF (1:1:2) solution. 56

4.8 Image of germanium wafer surface after 35 seconds of etching using $CuNO_3$ (10%) : HNO_3 : HF (1:1:2) solution. 57

4.9 Image of germanium wafer surface after 45 seconds of etching using $CuNO_3$ (10%) : HNO_3 : HF (1:1:2) solution. 58

LIST OF TABLES

1.1. Structural and thermal properties of germanium 2

1.2. Electrical properties of germanium and silicon. 5

1.3. Mechanical properties of germanium and silicon 6

2.1. Effective segregation coefficients (k_{eff}) of various dopants in germanium and silicon 19

3.1. Mechanical polishing steps. 36

3.2. Etching solutions applied during this study 39

4.1. Etching wafer identification and data 47

4.2. Average etching rates for different times..51

A.1. Visual Score and description used for blinded study 63

ACKNOWLEDGEMENTS

I would like to first acknowledge Dr. Sivaraman Guruswamy, Professor of Metallurgical Engineering and my advisor, for being so kind as to allow me to study under him and to obtain the education I received. I appreciate his patience and tireless effort in helping me finish my degree.

I am grateful for Sylarus Technologies, who took a chance on me out of school and allowed me to continue my education, and this work. I owe so much to the technical group that included Brian Lent, and Grant Fines who were gracious enough to tutor me and offer their knowledge on crystal growth; they did everything they could to make me a better engineer.

I would also like to thank my fellow graduate students who taught me so much more than I taught them.

Overall I owe so much to my wife, Emma, and my four children, who provide so much love and dedication. Without them, I wouldn't be where I am today.

CHAPTER 1

INTRODUCTION

Germanium was first postulated by Dmitri Mendeleyev in 1871, in his "theory of periodicity" and was later discovered in samples of a new mineral species, argyrodite (Ag_8GeS_6) by German chemist Clemens Winkler in 1886 [1]. Germanium is found in the group IV of elements on the Periodic Table of Elements with an atomic number of 32 and an atomic weight of 72.61amu. Its electron shell configuration is: $1s^2\ 2s^2\ 2p^6\ 3s^2\ 3p^6\ 3d^{10}\ 4s^2\ 4p^2$. Summarized in Table 1.1 are a number of germanium's important structural and thermal properties [2].

Germanium became well known in the 1940s as the first semiconductor with industrial use when it was used to build the first solid state transistor at Bell Laboratories. About a decade after germanium's rise, the first silicon transistor was introduced and silicon, because it was cheaper than germanium, has a higher bandgap, and has a stable native oxide, became the semiconductor of choice. A note of particular interest, when looking at the major differences between germanium and silicon, is the fact that germanium possesses the same crystal structure as silicon, i.e., diamond cubic, but the lattice constant of germanium is somewhat larger by 0.227 Å or 4%. With silicon reaching its limits in high frequency and nanocircuit devices [3], germanium is being looked at again with serious consideration as an active layer in advanced devices such as

Table 1.1. Structural and thermal properties of germanium.

Structural and Thermal property	Values for Germanium
Crystal Structure	Diamond (cubic)
Space Group	Fd3M
Lattice Constant	6.579060 Å
Crystal Density (at 300K)	5.3256 g/cm^3
Liquid Density	5.60 g/cm^3
Volume per Unit Cube	1.8112 x 10^{-22}cm^3
Atomic Density	4.471 10^{-22}cm^{-3}
Melting Point	1210.4K
Specific Heats (at 273.3K)	0.3295 J/gK (Cp), 0.3284 J/gK (Cv)
Thermal Expansion (at 300K)	5.90 x 10^{-6}K^{-1}
Thermal Conductivity (at 300K)	0.6 W/cm

IR optical apparatuses, radiation detection, MOSFETs, and multijuction solar cells. Seen in Figure 1.1 is the energy band structure for germanium, which is one of the most important characteristics of a semiconductor, especially those used for solar cells [4]. Semiconductors that are utilized for solar cells need to possess the appropriate band gap to absorb the solar spectrum efficiently. For multijuction solar cells, the band gap is also important because of the requirement for the semiconductor to be used in a junction configuration appropriate for controlling the electrical process involved in energy conversion. With its low band gap, germanium can be used as a substrate as well as providing an extra p-n junction to increase the overall cell efficiency [5]. Germanium also holds an advantage over silicon with its higher carrier mobility, which includes both hole and electron mobilities, as seen in Table 1.2. [2]. Germanium has more than twice the mobility of silicon at 300 K for electrons and four times the mobility for holes at the same temperature.

Though germanium holds many advantages electrically over silicon it is still vulnerable to the stresses, thermal and mechanical, that can be induced during crystal growth and the processing of wafers. Especially since germanium wafers used in multijuction solar cells are sliced ultrathin to reduce cost and weight, defects can cause cracking and catastrophic failure. When compared to silicon, germanium has a higher thermal expansion coefficient and density, and lower thermal conductivity. As seen in Table 1.3, these factors make it more susceptible to shear stress which can lead to nucleation and multiplication of dislocations and slip [6]. Germanium also has only a fraction of the Critical Resolved Shear Stress (CRSS), which is the stress required to initiate slip in a grain, near the melting temperature compared to that of silicon.

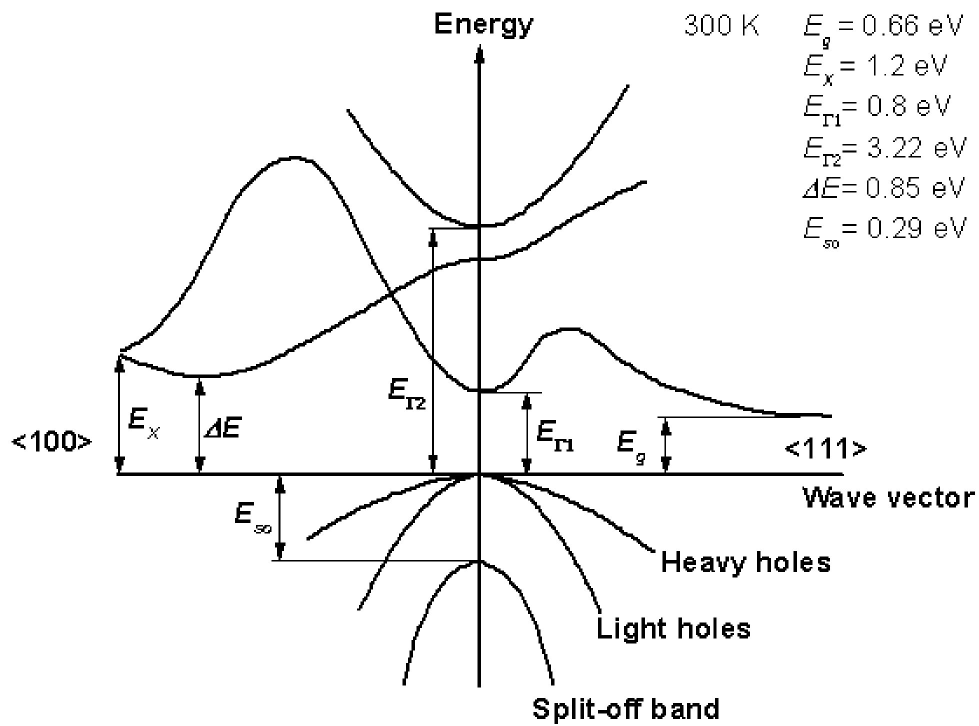

Figure 1.1 Energy band structure of germanium. Modified from Adachi [4].

Table 1.2. Electrical properties of germanium and silicon.

Parameter	Germanium	Silicon
Energy Band Gap	0.6657 eV	1.12 eV
Dielectric Constant	16.2	11.7
Electron Affinity	4 eV	4.05 eV
Electron Mobility at 300 K	3800 cm^2/Vs	1750 cm^2/Vs
Hole Mobility at 300K	1820 cm^2/Vs	450 cm^2/Vs

Table 1.3. Mechanical properties of germanium and silicon.

Parameter	Germanium	Silicon
CRSS at T_m (MPa)	1	4-8
CRSS at 0.7 × T_m (MPa)	110	7
Thermal Conductivity (W cm^{-1} °C^{-1})	0.58	1.3
Linear Thermal Expansion (°C^{-1})	5.9 × 10^{-6}	2.6 × 10^{-6}
Density (g cm^{-3})	5.32	2.33
Knoop Surface Hardness (kg mm^{-2})	780	1150
Mohs's Hardness	6	7

Chapter 2 discusses, in more detail, the causes of these stresses and opportunities for defect formation. Any defect incurred during growth and subsequent processing could compromise any electrical benefit that germanium may offer for device performance and reliability. For this reason, the detection of dislocations/defects is essential in developing a dislocation free crystal growth process as well as a wafer preparation process that does not promote defects in the material.

Preferential etching has been widely used in the investigation of defects in semiconductors and techniques and solutions have been documented to show plastic deformation in single crystal germanium grown by the Czochralski method [7-10]. This study reviewed those etching techniques and found them to be inadequate for p-type germanium crystals that are grown off the [100] direction towards the [111] direction, like those grown to match the lattice constant for gallium arsenide for multijuction solar cells. As a result, an etching solution and technique was developed to reveal dislocation etch pits, that correlate with defects, for the cross sectional face of gallium doped single crystal germanium that is grown in a direction between the angles of 4° to 8° off the [100] and towards the [111].

CHAPTER 2

SCIENTIFIC BACKGROUND

2.1 Czochralski Crystal Growth

The p-type germanium wafers used in this study were cut from single crystals grown using the Czochralski technique, also known as CZ crystal growth. CZ crystal growth is the most widely used technique for growing single crystal semiconductors because of relatively fast growth rates, capability to grow large diameters, and the ability to grow dislocation-free single crystals in an oxygen free environment. In fact, the CZ growth technique, founded by Teal and Little at Bell Laboratories and adapted from Jan Czochralski's method [11], was developed using germanium [12].

Figure 2.1 shows a growth assembly used to grow silicon crystals and is very similar to the apparatus used to grow the germanium employed in this study, except for a graphite crucible, and is consistent with many of the modern CZ crystal growers. The assembly includes a crucible to hold the melt where the crystal is grown from, a heater, and two mechanical systems, one to pull and rotate the crystal and the other to lift and rotate the crucible. Also important to a growth station, that is not shown, is a temperature control system to stabilize the melt temperature to allow growth off a seed, and a diameter control system.

Using the CZ method, the growth is started by charging, filling up, the crucible

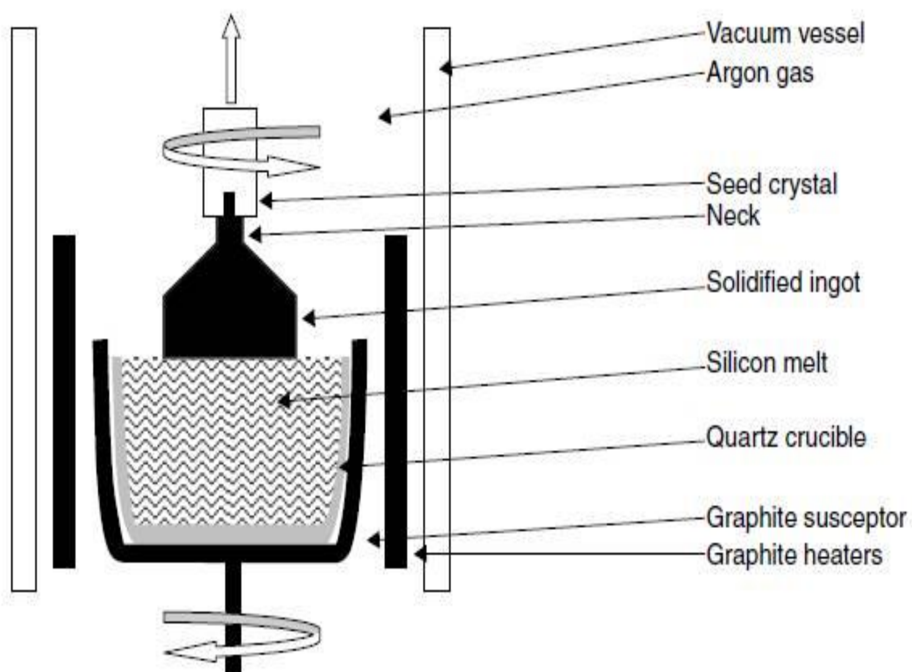

Figure 2.1 A sketch of the growth assembly for CZ crystal growth.

with the starting raw material. For semiconductors that easily oxidize at high temperatures, the puller chamber is pumped down to a high vacuum and an inert gas is flown through. The material is then melted down at a temperature above the material's melting temperature, see Table 1.1, for germanium. The crucible's height is then altered to obtain suitable temperature gradients (for both axial and radial directions) and the temperature is adjusted so that the melt's free surface center is marginally above the melting point. A seed, with the desired crystal orientation and free of defects, is then lowered and dipped into the melt. After thermal equilibrium is reached the growth process begins with the seed being pulled, and rotated, from the melt. The crystal diameter is controlled by the pull speed and temperature of the melt. When necessary, the crucible can be rotated to attain a cylindrically symmetrical thermal field in the melt. The crucible is also lifted to regulate the position of the free surface in relation to the heater top to gain optimal temperature gradients. An image of a germanium crystal grown by CZ method can be seen in Figure 2.2.

CZ crystal growth has many advantages over other growth methods, such as Bridgman and Float Zone techniques, which include its relatively quick growth speeds and most importantly, its large diameter growth ability. For years silicon has been grown with a diameter over 300 mm and reports of 200 and 300 mm germanium crystals grown from CZ have surfaced [13]. In addition, CZ crystal growth allows for observations during growth, permitting the process to be stopped and started over if complications, like the crystal becoming polycrystalline arises.

The germanium material used for this study was grown off the [100] towards the [111] to provide multiple and random lattice sites for high quality epitaxial

Figure 2.2 An image of a germanium crystal grown by CZ process.

growth used in multijuction solar cells. Figure 2.3 [14] outlines the [100], (110), and (111) planes for germanium, and Figure 2.4 [14], shows the crystal lattices for the three planes with the four-fold symmetry of the [100], two-fold rotation for [110] and three-fold symmetry for the [111].

2.1.1 Segregation in Crystal Growth

Alloyed and doped crystals are very common in crystal growth, where the dopants, or alloying elements, are supplemented in the crystal to produce specific properties. For the wafers used in this study, gallium was used as the dopant and was added in order to increase the free charge carriers of the crystals grown from the melt, making this a p-type semiconductor.

The concentration of elements in a doped crystal is generally not homogeneous because of the segregation or redistribution of the dopant from the major element atoms during crystal growth. The relationship between the concentration of dopant, or impurity atoms, in the growing crystal and that left in the melt is called the equilibrium segregation coefficient (k_o). The equilibrium segregation coefficient is calculated by:

$$k_o = \frac{C_s}{C_l} \tag{1}$$

where C_l is the concentration of the dopant in the solid, or crystal, and C_s is the concentration found in the melt. For segregation coefficients less than 1, the dopants are rejected by the solidifying crystal into the melt and are said to be tail end moving. Head end moving dopants have a segregation coefficient greater than 1 and the solubility of the

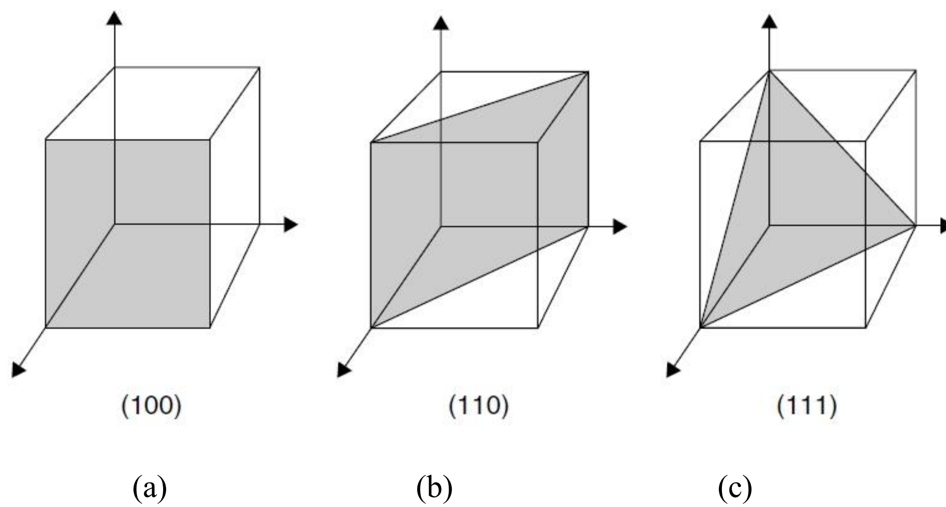

(a) (b) (c)

Figure 2.3 A sketch the (a) 100 (b) 110 and (c) 111 crystal planes in germanium single crystal. Reprinted from Introduction to Microfabrication, 2nd ed., S. Franssila, Silicon, pp 36-60. Copyright 2010, with permission from Elsevier [14].

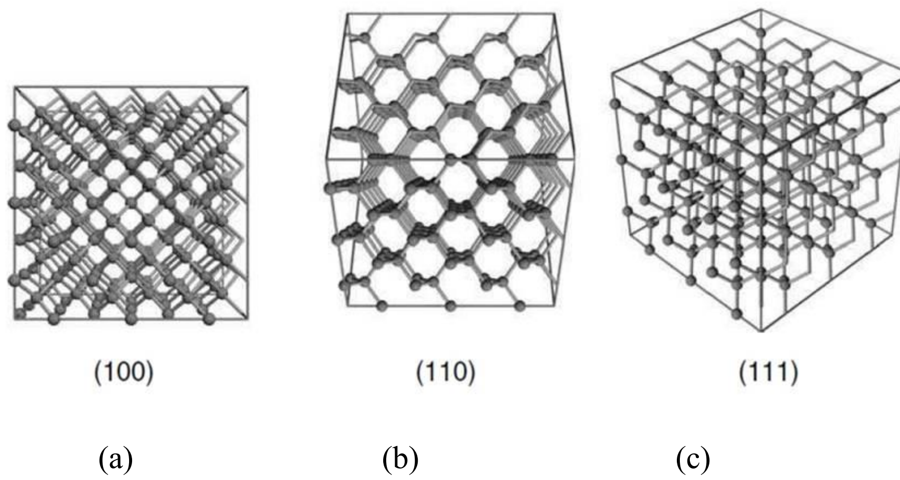

Figure 2.4 A view of the (a) 100 (b) 110 and (c) 111 atomic lattices in germanium single crystal. Reprinted from Introduction to Microfabrication, 2nd ed., S. Franssila, Silicon, pp 36-60. Copyright 2010, with permission from Elsevier [14].

dopant atoms are larger in the solid than in the melt. The driving nature of this segregation can be seen in phase diagrams like those shown in Figure 2.5 [15].

In both of these phase diagrams a small amount of impurity X is added to the pure elements A and B, respectively, and its percentage in the melt is represented by X_L. As the temperature drops to T_1 the two phases (solid and liquid) are in equilibrium with the concentrations X_L and X_S of the solute X in the two phases. The phase diagram on the left, in Figure 2.5 A, shows that as the melt reaches this temperature, T_1, the concentration of the impurity X in the solid (X_s) is less than in the liquid. This causes a rejection of the impurity atom into the melt and represents a $k_o < 1$. There is an opposite response in systems corresponding to the diagram on the right, in Figure 2.5 B, which has a $k_o > 1$ where the impurity concentration is greater in the solid than in the melt. A $k_o = 1$ would mean an equal distribution of the impurity during the liquid-solid phase transformation and a uniform distribution of the impurity along the length of the crystal.

As a note, the equilibrium segregation coefficients taken from phase diagrams do not always describe the redistribution effect in all crystal growth practices. Segregation depends on many growth kinetics like facetted vs. nonfacetted growth, pull rates, concentration levels of minor impurities, and thermal convections in the melt. Figure 2.6 shows how the segregation coefficient for antimony in germanium changes with different crystal growth axes [16].

The image also shows how the redistribution is a function of the crystal growth rate with k_o increasing as the growth rate increases. These nonequilibrium conditions lead to an effective segregation coefficient (k_{eff}) that describes the segregation of

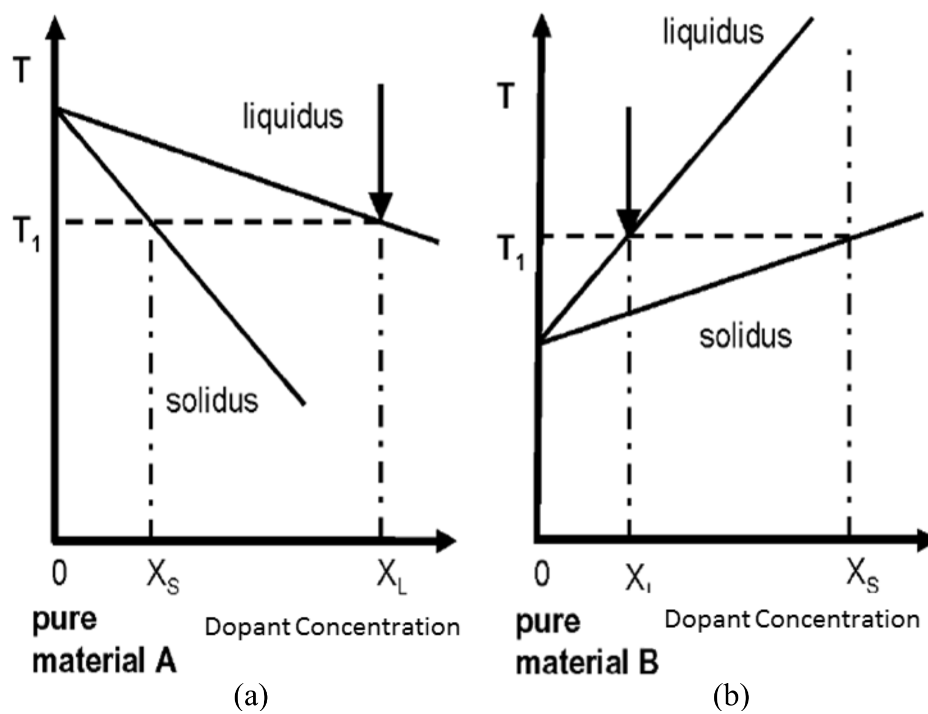

(a) (b)

Figure 2.5 Two distinctly different solvent-rich phase diagram regions that illustrate (a) segregation coefficient $k<1$ and (b) segregation coefficient $k>1$. Modified from Muller [15].

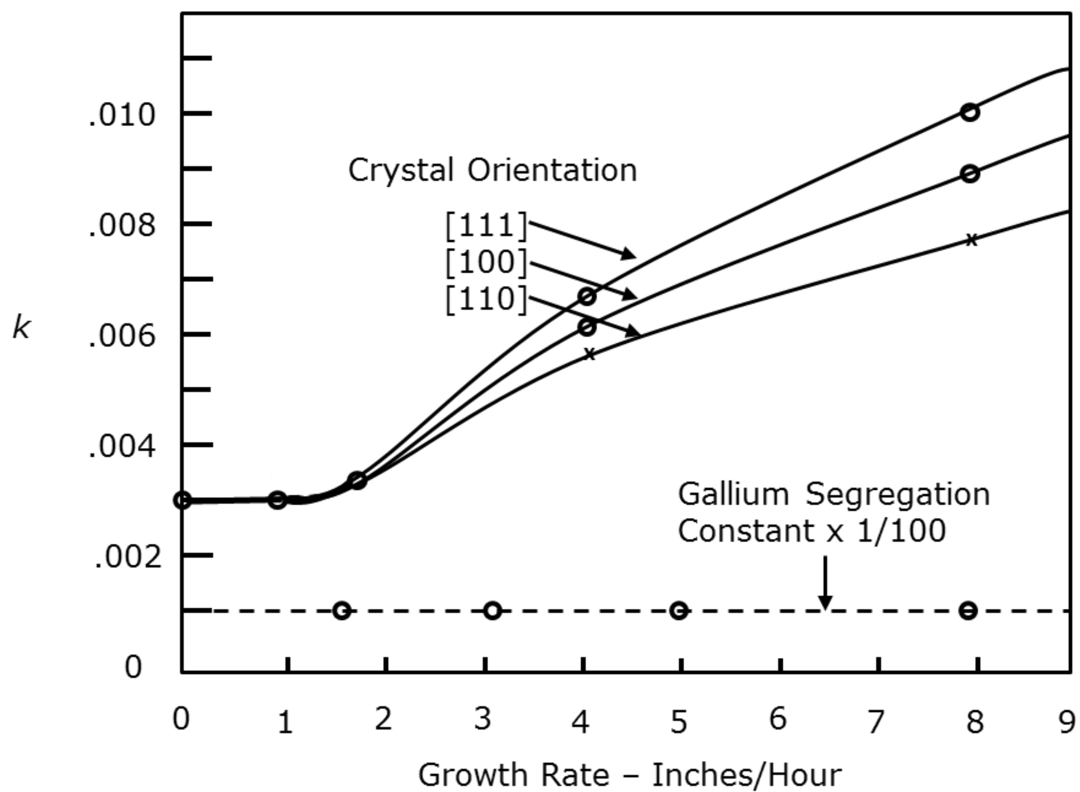

Figure 2.6 Variation of effective Ge segregation coefficient as a function of growth rate. The segregation coefficient for gallium in germanium is included for comparison. Modified from Hall [16].

impurities under effective segregation coefficient (k_{eff}) that describes the segregation of impurities under actual growth performances and is not theoretical. Table 2.1 shows some effective segregation coefficients of dopants in germanium and silicon, including gallium, which is tail end moving for both elements.

Figure 2.7 shows a schematic curve of a growing crystal and the impurity distribution at the solid-liquid interface for k_o <1 [17]. With the rejection by the growing crystal, the concentration of the impurity atom in the melt becomes higher just at the solid-liquid interface compared to that in the volume of the melt. In the case where T_A is below T_E, as seen in Figure 2.8, where the melt temperature is lower than the actual thermodynamic equilibrium (liquidus) temperature, there exists a region in-between of supercooled melt [17]. This brand of supercooling is called constitutional supercooling because it occurs from the constitution, or composition, of the melt and build up of impurities at the solid-liquid interface for dopants like gallium, which has a k_o <1 in germanium.

Constitutional supercooling is detrimental in crystal growth because of the instability at the solid-liquid interface. Dislocations can generate due to buildup of impurities at the interface and the nonuniform concentration in the melt causes a radial discrepancy of the solid and melt temperatures. This disparity in the temperatures can cause alterations in the interface shape, which can also propagate dislocations because of stress in the atomic lattice. There is also the risk, from the nonuniformity, for the collapse of single crystal growth resulting in a cellular structure or polycrystalline material [18].

Table 2.1. Effective segregation coefficients (k_{eff}) of various dopants in germanium and silicon.

Element	**Germanium**	**Silicon**
Lithium	0.002	0.01
Copper	1.5×10^{-5}	4×10^{-4}
Aluminum	0.073	0.002
Gallium	**0.087**	0.008
Silicon	5.5	1
Germanium	1	0.33

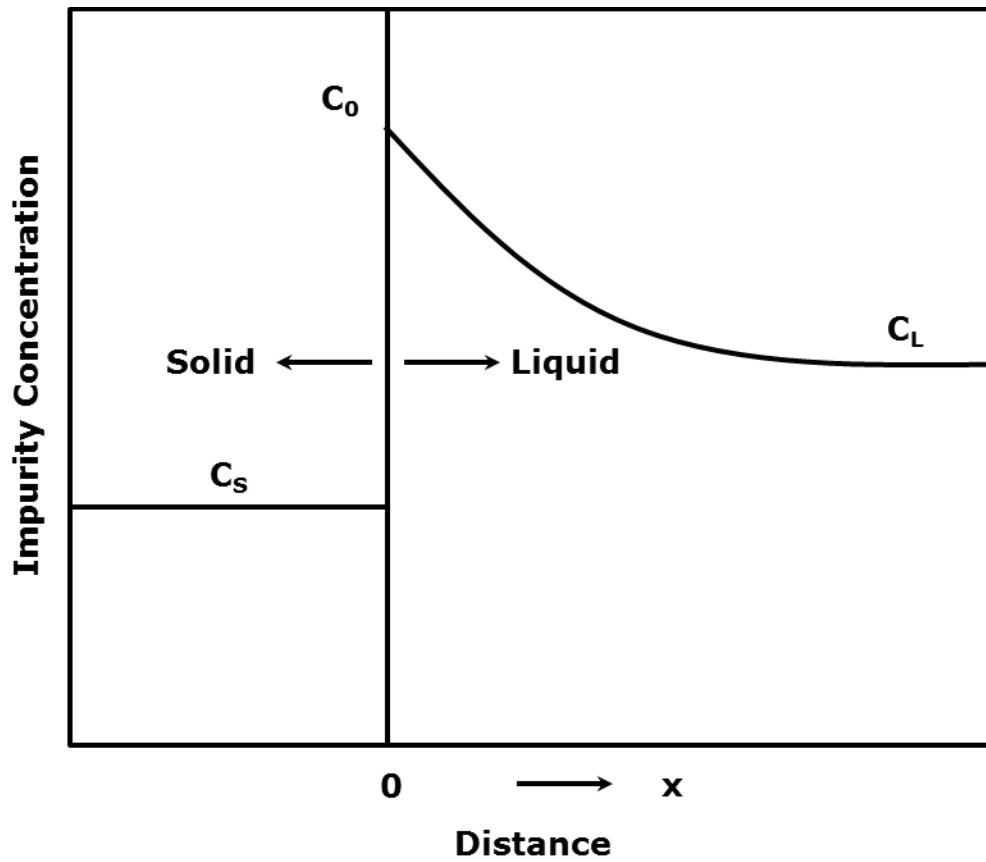

Figure 2.7 Schematic curve showing the impurity distribution across the solid-liquid interface for k_o <1. Modified from Kodera [17].

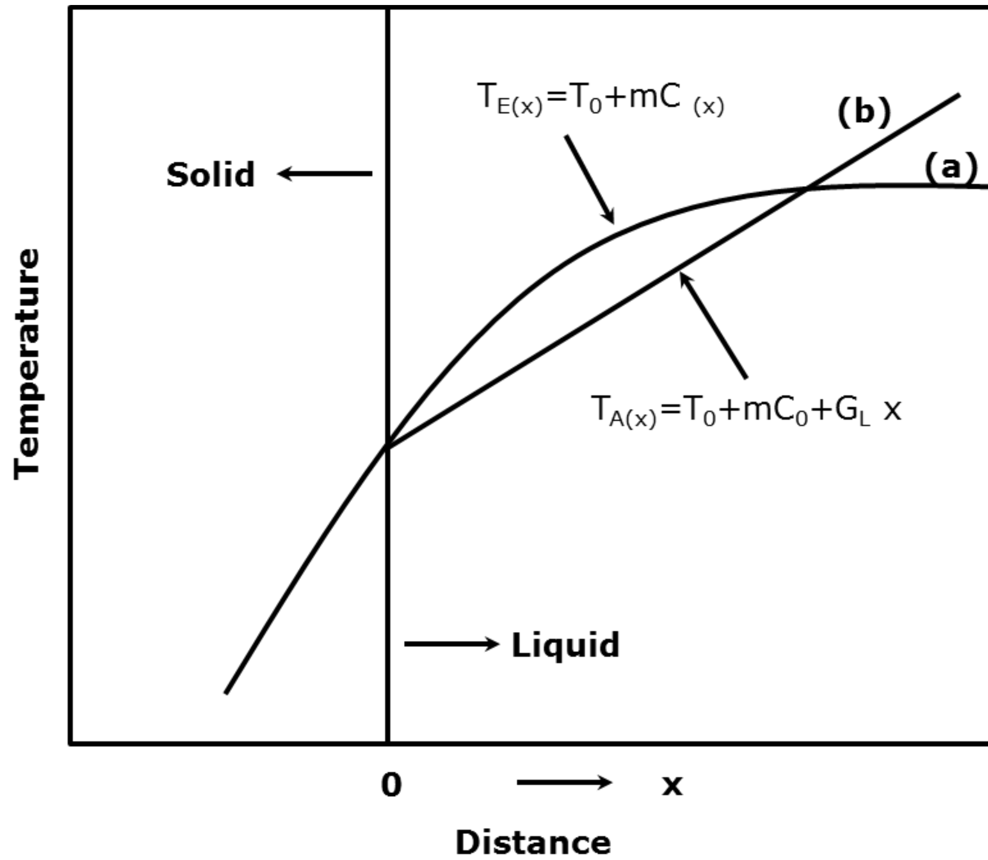

Figure 2.8 Schematic curves showing the temperature distribution across the solid-liquid interface for k_o <1; (a) melt temperature; (b) actual thermodynamic equilibrium liquidus temperature. Modified from Kodera [17].

2.1.2 Thermal Stresses in Crystal Growth

Though CZ crystal growth holds many advantages over other growth techniques, there are still many parameters that need optimization in order to produce dislocation-free material. The thermal properties in a crystal growth system are one of those major parameters that need appropriate attention for all techniques of crystal growth, including CZ.

Due to the nature of crystal growth, high temperatures are required in order to melt and sustain molten material before and during solidification. The temperature differences, or gradients, throughout the entire system can cause thermal stress in the growing and cooling crystal that can generate dislocations. In fact, the major reason for dislocation generation in crystals growth is because of too high thermal stresses in the material. In the case of the germanium wafers used in our research, and illustrated in Table 1.3, the thermal and mechanical properties of germanium hold the disadvantage, compared to silicon, for dislocation-free crystal growth.

One of the sources of thermal stress in a growing crystal is the occurrence of a radial temperature gradient across the solid-liquid interface, as seen in Figure 2.9 [19]. In this figure T_M is the melting temperature of the material and temperatures T_1 and T_2 illustrate a decrease in temperature as you move up and towards the middle of the crystal. It is this radial temperature gradient that is principal to an increase of thermoelastic stress at the edge of the crystal. Application of a temperature gradient puts the hottest part of the crystal under compression and the coldest part under tension. Such plastic bending equates to the introduction of a number of edge dislocations with a density (n) equaling:

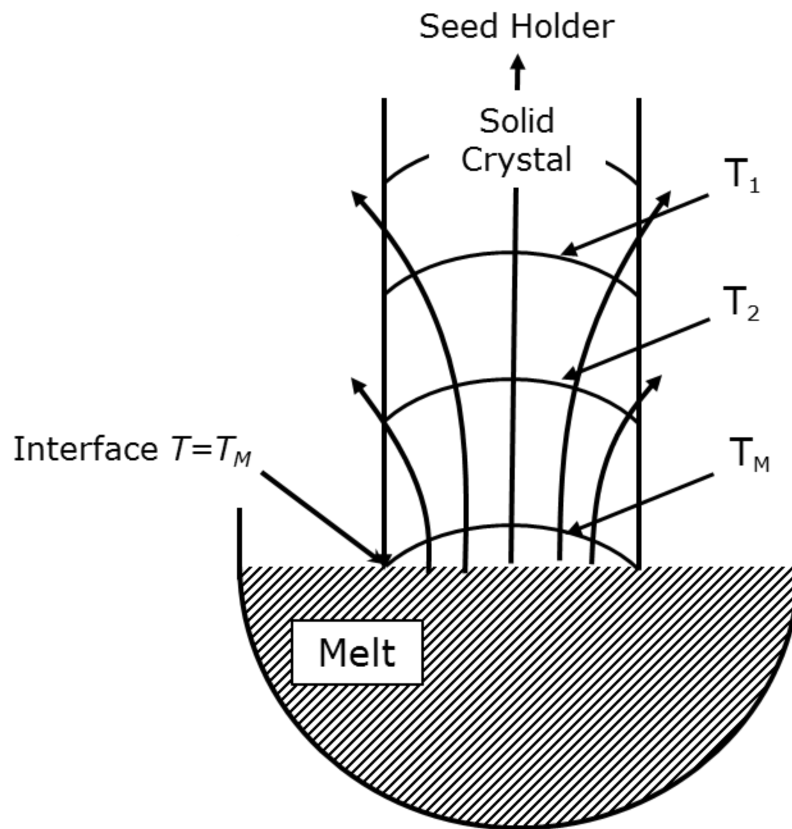

Figure 2.9 A schematic diagram illustrating the radial and axial temperature gradients in a single crystal being pulled from the melt. Modified with permission from The Royal Society of London. Billig, E., "Some defects in crystal growth from the melt," Figure 1 pp. 40, Proceedings of the Royal Society of London, Vol. 235, No. 1200, 1955 [19].

$$n = \frac{\alpha_e}{b} \frac{\delta T}{\delta r} \quad (2)$$

where *b* is the length of Burgers vector of the dislocation, α_e the linear expansion coefficient, and $\delta T/\delta r$ the radial temperature gradient [19]. Moreover germanium is denser as a liquid than as a solid (~5) so as the atoms in the melt join the crystal and freeze there can be a generation of defects at the highest thermal gradient points (i.e., the top, the bottom, and the edge). Figures 2.10 and 2.11 show low angle grain boundaries near the edge of germanium wafers.

Along with the temperature gradient in the radial direction there abides an axial temperature gradient during growth and throughout the cooling of the crystal, as seen in Figure 2.9. As mentioned before and seen in Table 1.1, germanium is less dense as a solid than as a liquid so there is an expansion of the crystal as it cools by an amount ε, given by:

$$\varepsilon = \alpha_e \Delta T \quad (3)$$

with ΔT being the temperature difference from solidification to equilibrium temperature [20]. Such expansions can generate dislocations as stress builds up in the atomic lattice and the Gibbs free energy increases. There are not only thermal stresses involved in

the solid material, being held by the seed, tensile stress is also increasing at a rate proportional to the growth rate. Table 1.3 shows the critical resolved shear stress (CRSS) for germanium

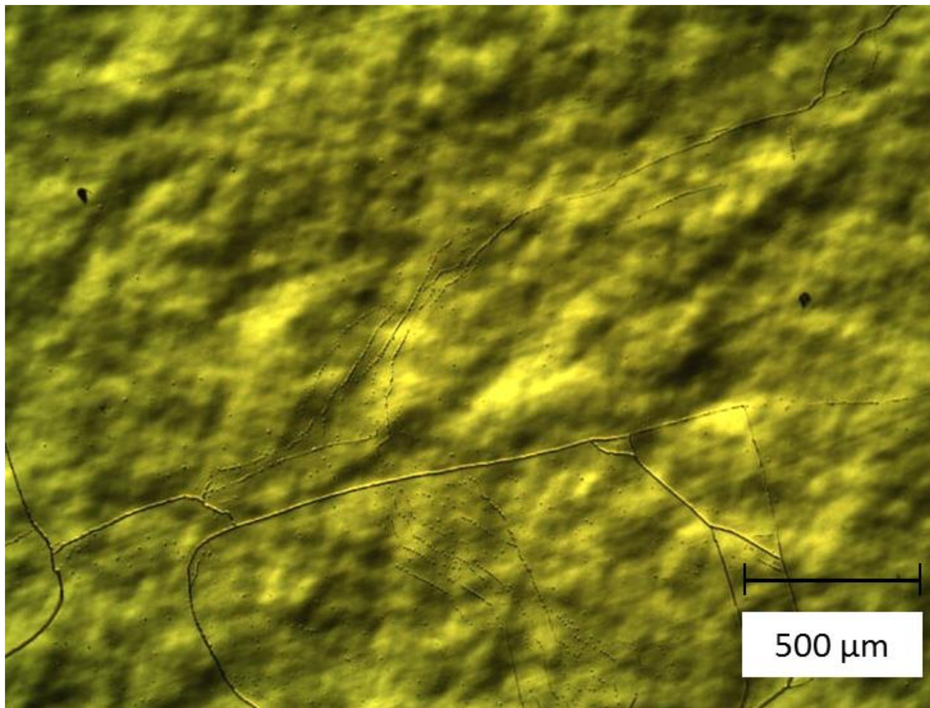

Figure 2.10 Optical micrograph of a preferentially etched germanium wafer revealing low angle boundary dislocations.

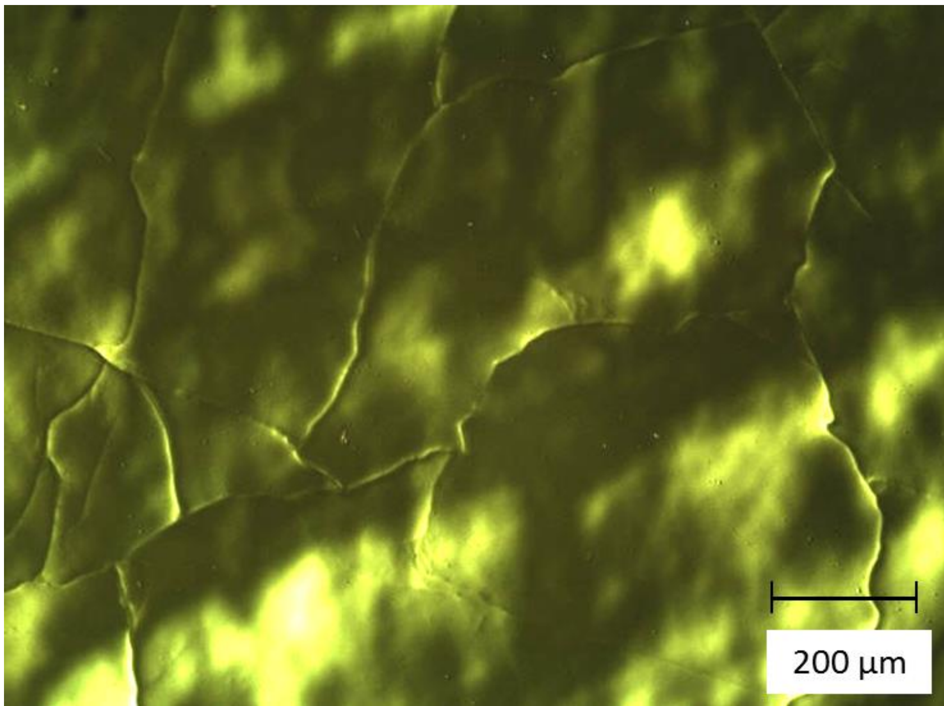

Figure 2.11 Optical micrograph of a preferentially etched germanium wafer revealing low angle boundary dislocations and cellular structures.

and silicon, which is the breaking point for stress values for the creation of dislocations in the material. Germanium has a lower CRSS than silicon which means it has a higher probability of dislocation nucleation and propagation compared to that of silicon. There have also been some studies that have shown that dislocations in germanium, in relation with plastic flow and material strength, show a much higher dislocation mobility compared to silicon [21].

As mentioned in this section, and in the previous one, there are numerous possible causes of the generation of dislocations during CZ crystal growth of germanium. Some of these are impurity microsegregation due to constitutional supercooling, too high thermal stresses caused by temperature gradients, and thermal and mechanical shocks from expansion. Some causes not mentioned include a solid-liquid interface deflection (both convex and concave), inclusion of gases or solid particles at the interface, and melt vibrations from outside sources. All these probable causes show the sensitivity of the crystal growth process, particularly for germanium. With a need for defect free germanium to be used for epitaxial growth, it is necessary for one to be able to test successful growth parameters by examining the quality of crystals produced and the possible defects laid in from growth.

2.2 Germanium Wafer Processing

Germanium crystals, or ingots, are converted into wafers by way of a multistep process which includes several mechanical and chemical treatment steps. There are also many cleaning and inspection steps throughout the process of creating the wafer. The chief steps in the wafering process are described below and illustrated in Figure 2.12 [22]

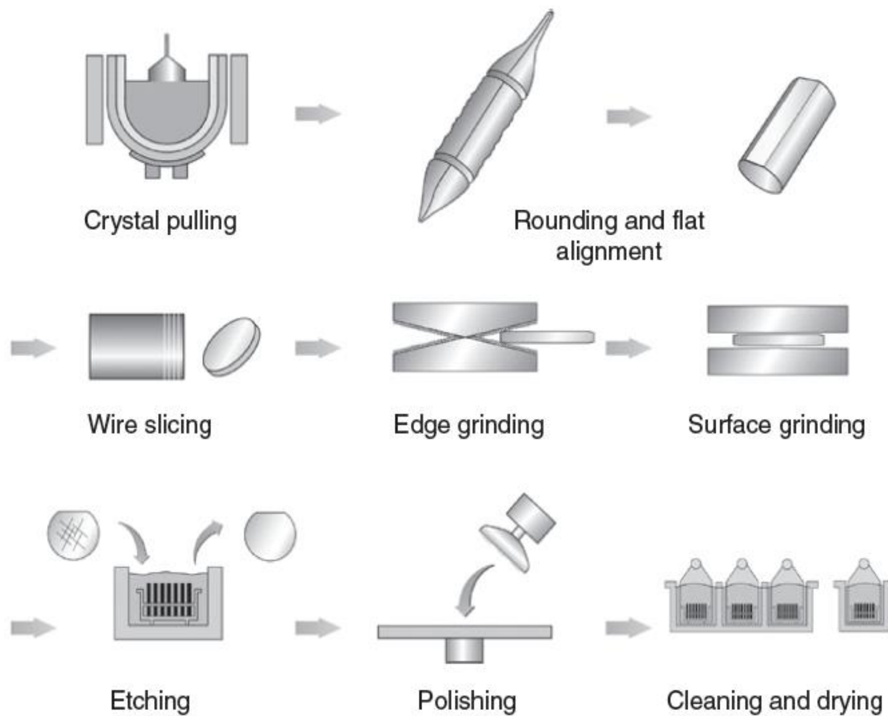

Figure 2.12 Flow chart for the germanium wafer production process. Reprinted from Germanium-Based Technologies From Materials to Devices, C. Claeys and E. Simoen, Germanium Materials, pp 11-40. Copyright 2007, with permission from Elsevier [22].

After the growth and cool down of the crystal is completed, the crystal is removed from the puller and the crown and tail (top and bottom) are removed by wire or Outer Diameter (OD) saw. The crystal is then turned down by mechanical grinding to slightly larger than the desired wafer size and a flat is put on to identify the wafer orientation. Some materials other than germanium may have a secondary flat that helps with classifying orientation and doping type. The transformation from bulk crystal to wafers is made during the wire slicing procedure, where the ingot is slowly pushed through a web of thin steel wires carrying slurry of small abrasive material. The wafer is then marked with a laser and ground on the edge and surface before being etched to relieve any internal stress. At the end of the process the wafer is polished on one side, to remove any subsurface damage and provide a smooth surface for epitaxial growth, then cleaned, dried and packaged.

It is during the multiwire slicing where the wafer undergoes a majority of the mechanical damage during the wafering process. Because germanium is brittle at lower temperatures, damage is induced on both sides of the wafer as the abrasive material pushes against the germanium crystal until atoms are sheared off along certain planes and a cut is made. What is left after the wire has passed the wafer is subsurface damage consisting of fractures, microtwins, and dislocations [23]. Figure 2.13 [24] illustrates the layers of subsurface damage on a wafer after slicing and the depth that some damage can reach. Looking again at Table 1.3, germanium has a lower hardness value compared to that of silicon and is therefore more susceptible to scratching and subsurface damage from abrasive particles. Deformation from edge and surface grinding, polishing, and handling of the wafers can also induce stress on the atomic lattice that can lead to

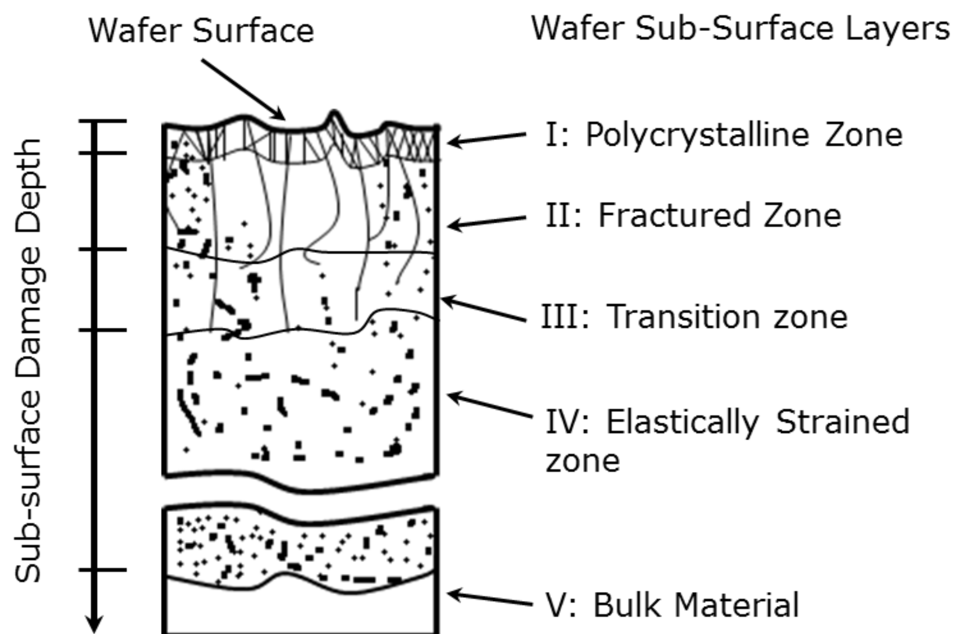

Figure 2.13 Subsurface damage of a wafer after slicing. Adapted from Hadamovsky [24].

propagation of cracks on cleavage planes beyond the contact zone and into the bulk material.

These defects can be damaging or lead to catastrophic failure of the wafer due to the fact that many of the devices these wafers are utilized in require Chemical Vapor Deposition (CVD) of III-V type alloys grown on them. Any defect, or cracking, will result in the uneven growth of these additional layers which may lead to the failure of the wafer and its ability to perform as needed.

Though polishing and chemical etching of the wafer is meant to take away the damage from previous process steps, some defects may reside if the damaged area is not removed or defects propagate into the bulk material. Preferentially etching the wafer can reveal residual damages and aid in honing variabilities in processes that eliminate any subsurface damages induced by the wafering practice.

2.3 Dislocation Etch Pits

When a solid crystal is exposed to an undersaturated atmosphere, or some other corrosive environment, it experiences a reaction that is called decrystallization, or dissolution etching. This process is sometimes called chemical milling because layers of atoms are removed from the surface causing a reduction in mass and thickness of the material. At certain points on the surface of the crystal the etching process may be more rapid than at other points, which can lead to nonuniformity in the remaining surface, this is called selective etching. For a low index surface, sites where defects intersect the observed plane of the crystal are specific points where selective etching takes place and leads to the formation of pits. An example can be seen in Figure 2.14 which has an

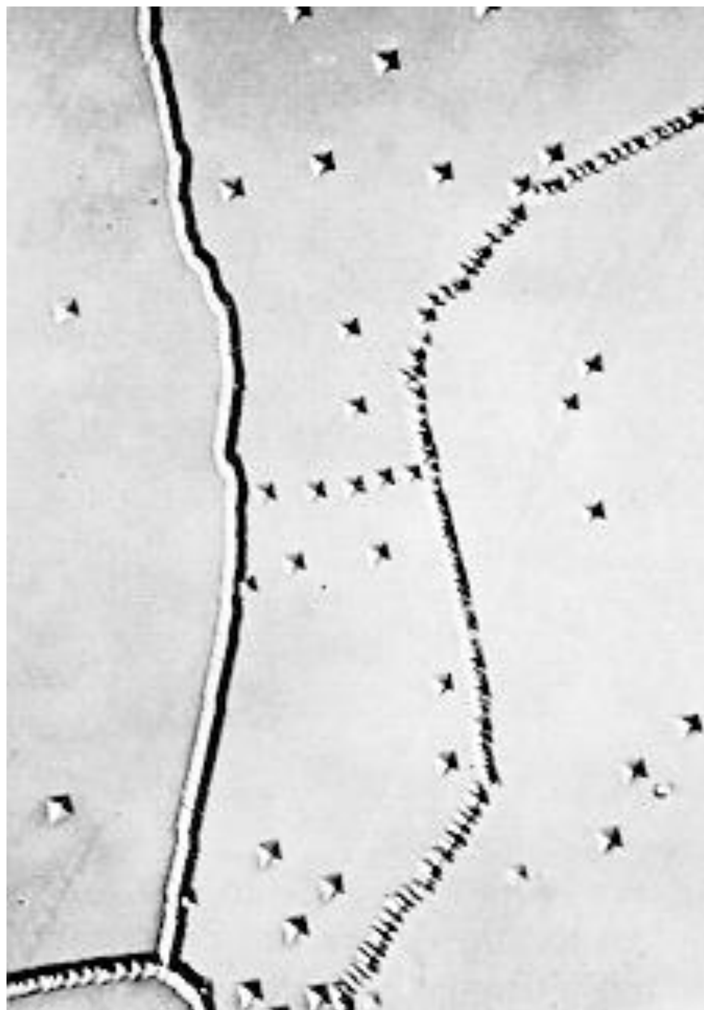

Figure 2.14 Etch pits in LiF single crystal. Reprinted from Muller [15].

inverted pyramid shape. These etch pits can be viewed using microscopy tools like a light microscope that possessed Normarski Differential Interference Contrast (DIC) capability used for Figure 2.14.

Vogle, Pfann, Corey, and Thomas from Bell Telephone Laboratories proved that there is a 1:1 correlation linking etch pits in germanium and dislocations seen from selective etching and is therefore a valuable tool in mapping and understanding defects in germanium [25]. As mentioned before these dislocations in germanium are caused by strain on the crystal from either thermal stress of growth or impurities trapped in lattice sites as well as impact on the material from the wafering process. These stresses in the crystal lattice accelerate the rate of nucleation of pits due to the energy localized at the defect site and the result is the formation of voids, or pits. The geometrical shapes, like those seen in Figure 2.14 are due to close-packed planes in the crystal structure, the (111) in germanium's case, that binds the planes like the (100) that etch more easily [15].

2.3.1 Chemical Etch Solution for Revealing Dislocations

There are multiple techniques used to distinguish and reveal dislocations and determine the density of crystals defects. Some examples include: thermal etching; electrolytic etching; preferential oxidation; or an application of a chemical etch solution. Of those mentioned, the use of a chemical etch solution is the simpliest and most commonly used method.

The chemical etch solution, or dislocation exposing solution, is applied to an appropriately prepared sample by surrounding the desired surface, or entire sample, until the dislocations are exposed.

There has been multiple etching solutions studied and published to selectively etch single crystal germanium and reveal defects with pits. Some of them are marked as a general solution etchant, but most of them are tagged for a specific crystal orientation for the surface of the crystal. None of them are designed to preferentially etch germanium grown off the [100] towards the [111] between angles of 4°and 8°.

CHAPTER 3

EXPERIMENTAL PROCEDURES

3.1 Sample Preparation

P-type germanium wafers, from single crystals grown using the Czochralski technique and oriented 4°-8° off the [100] plane towards the [111] plane, were cut perpendicular to the axis of crystal growth and utilized in this study. The primary surface state of the wafers was irregular, because up to this point the wafers had only gone through the process steps, described in Section 2.2, of crystal growth and cropping of the head and tail. After the head and tail were cropped an additional section, ranging from 1-2 mm thick, was cut for this study.

Wafers were then cleaned utilizing a two-step process. The first step applies a solvent, a mono-substituted benzene derivative, on the wafer in order to remove any adhesives, petroleum products (cutting solution), and abrasive material that may be left on the wafer. The samples were then cleaned using isopropyl alcohol, to dissolve any remaining oils and remove any residual products. Isopropyl alcohol is also miscible in water and easily removed during the polishing process.

After cleaning, wafers were polished in order to remove any surface damage that may be induced during the cutting process, see Figure 2.13. The germanium samples were mechanically polished following the steps found in Table 3.1. The 600

Table 3.1. Mechanical polishing steps.

Grit-Type	Minimum Removal
600 - Paper	100 μm
1200 - Paper	100 μm
6 μm – Diamond Paste	50 μm
3 μm – Diamond Paste	18 μm
1 μm – Diamond Paste	9 μm
1 μm – Al Paste	3 μm
0.3 μm – Al Paste	1 μm
0.05 μm – Al Paste	0.5 μm

grit paper is used in order to remove enough material from the surface as to reach the "bulk material" and eliminate any subsurface damage left over from the cutting of the sample. The subsequent steps are employed in order to remove the damage laid in from the previous grit size; with the end result being a smooth surface with little to no damage from the polishing process and an opportunity to explore defects laid in from growth. An image of a polished germanium wafer is shown in Figure 3.1.

3.2 Etching Solutions

Table 3.2 shows the different etching solutions for germanium tested during this study. Although these etching solutions did work to chemically mill the germanium wafer, by removing material from the surface, none were effective in revealing the etch pits needed for marking dislocations in the material in the respective growth direction. Figure 3.2 shows the typical results seen from etching the germanium wafer with the solutions found in Table 3.2; the surface is irregular and the structures appear to be more like hillocks than pits.

3.2.1 Solution Discovery

Over the course of a year, several near <100> oriented wafers were cut, polished, and then etched with many of the common etchant solutions used for germanium with little success. Over 50 samples were utilized in this study. For etching of the off-axis grown towards the <111> material, etching solutions published for planes between the Z axis and the <111> for germanium were explored. After an extensive literature study, on etchant solutions, a report from the Lawrence Berkley (LBL) was found where a study was carried out to comprehend the electrical properties

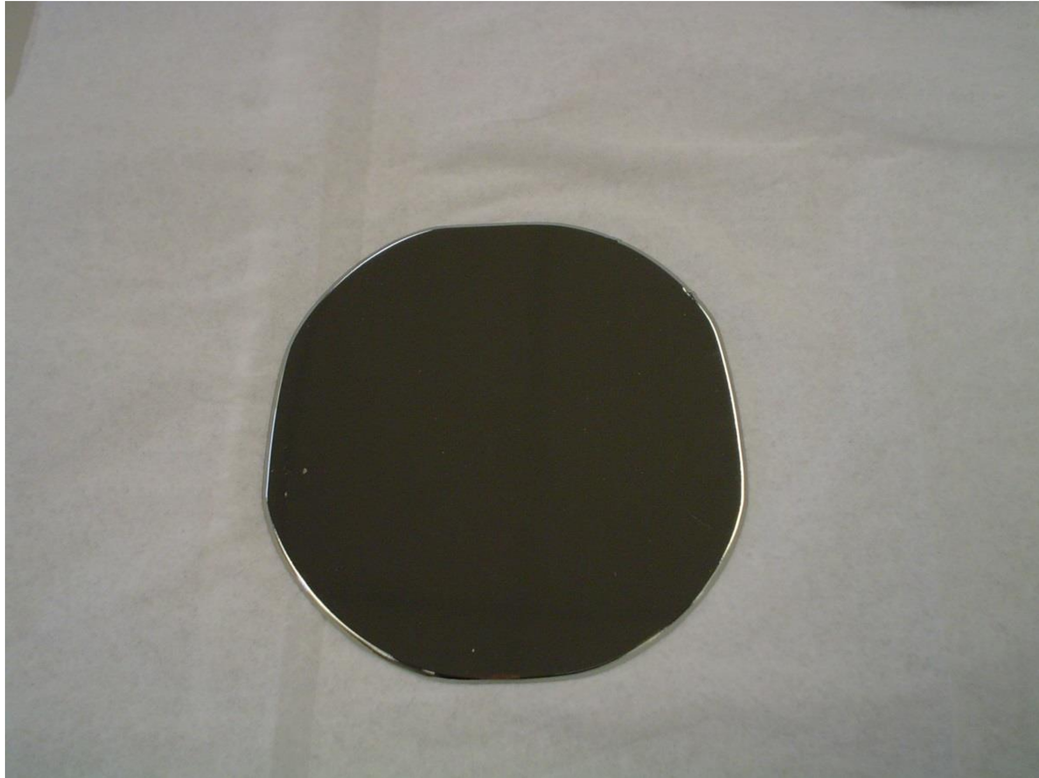

Figure 3.1 An image of a polished germanium wafer.

Table 3.2. Etching solutions applied during this study.

Etchant	Solution
#1	HNO_3: HF : Acetic Acid: (5g/10 ml H_2 solution) [5:3:3:1]
#2	5cc HF : 11cc Acetic : 10 cc HNO_3 : 30 mg I_2
Potassium Iodine	2000 mg KI : 200 mg I_2 : 50 ml H_20
WAg	HF : H_20_2 : 5% $AgNO_3$ [4:2:4]
Superexol	HF : H_2O_2 : H_20 [1:1:4]
CP-4	HF : Acetic : HNO_3 : Br_2 [5:3:3:0.1]
#3	HF : H2O2 : H20 [1:1:64]

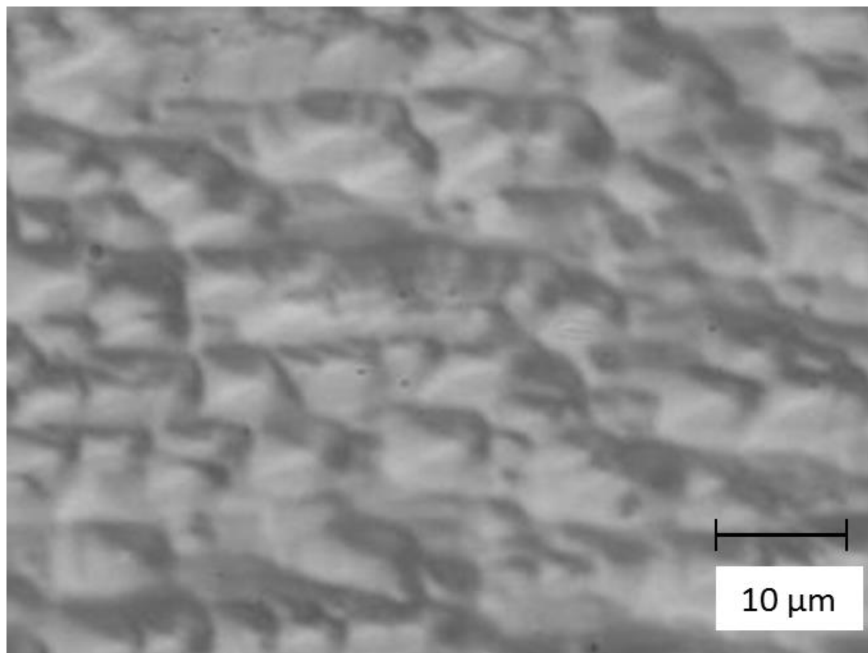

Figure 3.2 Wafer surface after etching with Superexol for 75 seconds.

of dislocations in ultrapure germanium [27].

The material used by LBL's study was single crystal germanium grown by the Czrochralski method in the [100] and [113] directions. They reported that an etching solution of $CuNO_3$ (10%) : HNO_3 : HF (1:1:2), was used for 1 minute for material cut perpendicular to the [100] and revealed etch pits. For those materials grown in the [113] direction a solution of $CuNO_3$ (10%) :H_2O_2:HF (1:1:2) was used for 6-10 minutes.

3.2.2 Etch Process

The process by which the germanium samples were etched in the study by LBL was not described [27]. For the testing of solutions a similar process as described by Ehman where their "etching was carried out in the appropriate solutions with mild agitation for periods of 15 seconds to 1 minute in a teflon basket at room temperature"[28] was employed in this work. Instead of teflon our germanium wafers were placed in a pyrex cylinder, with a diameter slightly larger than the wafer, and agitated in a clockwise motion as the solution was poured over it. The agitation was employed in order to achieve a uniform etch rate over the germanium surface.

To terminate the etching a liter of Deionized (DI) water was poured into the cylinder, at the designated time, and then followed up by a constant rinse of DI water for a minimum of 30 seconds using a hand spray tool.

The reporting periods included times from 5-45 seconds, though testing was done for longer optimal times and were found to be between 35-45 seconds. We only report on these values here. Two-hundred ml of etching solution was used for each wafer and all etching was conducted at room temperature and within ventilated fume hoods.

3.3 Evaluation of Dislocations and Density

All surfaces, etched and unetched, were observed under a Nomarski Differential Interference Contrast Microscope and images taken with an attached digital camera. Etch pits were also observed using the bright-field mode, on the optical micrsoscope, where the etch pits appeared as black dots and the rest of the surface looked white. The dislocation etch pit density of the samples were calculated manually; two orthogonal lines, on the wafer, outlined the sampling area and 5 measurements were taken along each of those lines, for a total of 10 appraisals. The values where then added up and then averaged, a scale factor, for the magnitude, was then applied to the average.

3.4 Etching Solutions

Before the crystals used in this study were sliced and made into wafers, their crystallographic orientations were verified using a 2-Theta X-ray Diffractometer. Subsequently each of the 30 wafers used in our experiment had their orientations checked to ensure there was no misalignment due to the cutting process.

CHAPTER 4

RESULTS AND DISCUSSION

4.1 Etch Pit Results

The solution of $CuNO_3$ (10%):H_2O_2: HF (1:1:2), used by Haller et al. at LBL for germanium with [113] orientation, was used to etch the single crystal germanium in our study [27]. Haller et al. reported that a time of 6-10 minutes was used, though they never experimented with any times beyond 6 minutes due to the severe exothermic reaction of the solution with germanium. Initial test results showed some etch pits on the wafer but the solution was inconsistent in replicating the results on all wafers. The solution was more reliable while etching wafers from the head end of a crystal, where low angle grain boundaries were more prevalent and the dislocation density was higher, compared to the tail end.

Because a reliable solution was being sought it was decided that we try the solution reported for germanium grown on the [100]. This solution, $CuNO_3$ (10%): HNO_3 : HF (1:1:2), resulted in more distinct and clear etch pits compared to that for the [113] solution. Etch pits were visible after those that were etched >15 seconds, and proved to be repeatable for both head and tail end wafers. Figure 4.1 shows the pyramidal etch pits seen using this solution; the <111> faces are seen along with the four-fold symmetry of the growth axis. Though the reported time to etch germanium,

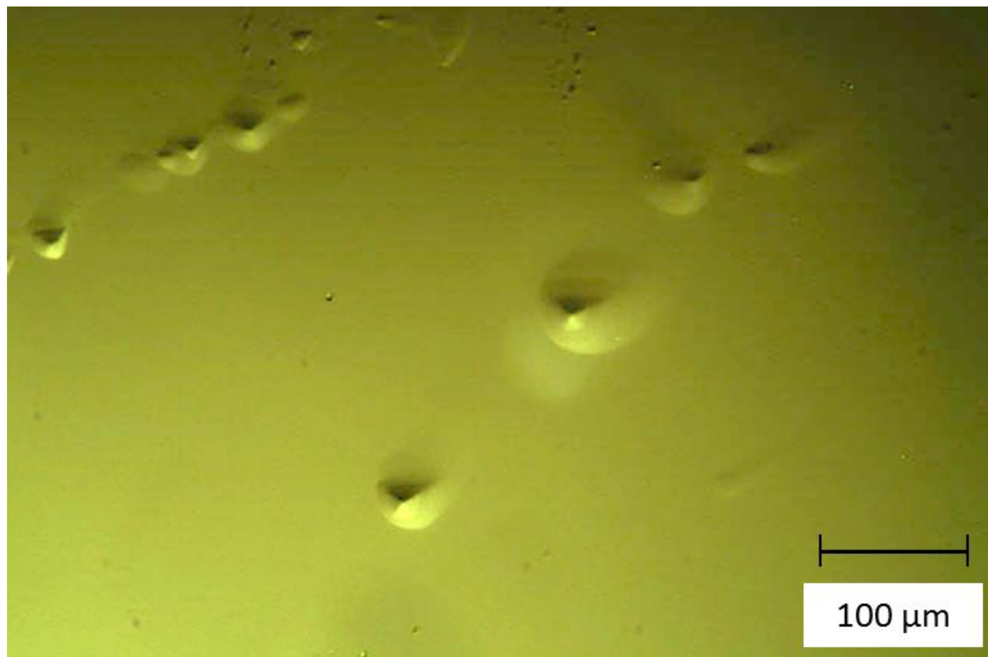

Figure 4.1 Etch pits on a germanium wafer.

using this solution, was 1 minute, we found that an etch time of 45-50 seconds was adequate to reveal etch pits and still preserved the surface of the material without over etching.

It is likely this solution was more successful due to the fact that the plane being etched is closer to the <100> axis, by 4°-8°, compared to that of the <113> direction, which in itself is 25.24° from the <100> and would be 17.24°-21.24° from the plane of the material. Due to the positive results and production environment of this study, the $CuNO_3$ (10%) : HNO_3 : HF solution was studied in more detail and is the subject of the remainder of this work.

4.2 Etching Rates and Times

Etch rates of the solution, $CuNO_3$: HNO_3 : HF, were determined by the thickness difference of the wafer before and after submersion in the etch solution. Thickness values were measured using a pair of Mitutoyo digital micrometers with a resolution of $1x10^{-3}$ mm. Due to the vapors released from the solution, which began a few seconds into the etch, the temperature was measured on the surface of the Pyrex container in which the etching was carried out. Because of the high thermal conductivity of Pyrex® glass it is assumed that the surface of the glass is relatively close to the temperature of solution it houses and therefore the temperatures during etching. The temperature was measured using an Omega® infrared thermometer with a resolution of 1.7° C.

A blind study was designed where times of 5, 15, 25, 35 and 45 seconds were chosen for the study and each time was replicated 6 times. Thirty wafers, 15 from the

head and 15 from the tail, were labeled from A-AD and were chosen at random for each time interval test. Because the prior etchant seemed to reveal dislocations on the head end more consistently than the tail end, the origin of each wafer location, with respect to the crystal, was blinded until after the study as to not bias those who were looking and recording results. A visual score system was created in order to evaluate the effectiveness of each test time, the values and definitions can be seen in the Appendix. Table 4.1 shows the results from the test, which includes Wafer ID, material removed, etch rate, temperatures and visual score of each recorded time.

Initial etch rate calculations were arranged to account for removal of germanium only on one side, the top face, of the wafer due to the etch process. During pretrial tests, it was observed that there was etching across the whole surface of the bottom face of each wafer which meant that both sides were being chemically milled. It was witnessed that the wafer became suspended in the solution during the etching due to the agitation and in part to fumes being released from the solution. As the temperature increased the solution began to boil and the fumes actually pushed the wafer up towards the top of the solution. Because of this phenomena the etch rate equation was altered in order to accommodate etching on both sides. The average etch rate per side is estimated by taking the total thickness reduction and dividing by 2. The etch rate, per minute, is calculated by the following formula:

$$Rate = \frac{t}{60} * \frac{\Delta d}{2} \quad \mu m/min \tag{4}$$

Table 4.1. Etching wafer identification and data.

Wafer ID	Time (Sec)	Removal (μm)	Rate (μm/min)	Temperature (C°)	Visual Score
G	5	10	0.42	26	1
H	5	10	0.42	28	1
Q	5	15	0.63	27	1
R	5	10	0.42	26	1
AA	5	15	0.63	27	1
AB	5	15	0.63	26	1
E	15	35	4.38	38	2
F	15	30	3.75	40	1
O	15	35	4.38	39	2
P	15	35	4.38	39	2
Y	15	30	3.75	38	2
Z	15	35	4.38	39	2
A	25	75	15.63	58	3
B	25	70	14.58	60	4
K	25	80	16.67	59	4
L	25	75	15.63	57	3
U	25	80	16.67	57	4
V	25	75	15.63	56	3
I	35	125	36.46	75	5
J	35	120	35.00	72	4
S	35	115	33.54	73	5
T	35	120	35.00	75	5
AC	35	115	33.54	76	5
AD	35	115	33.54	73	5
C	45	165	61.88	93	5
D	45	160	60.00	95	5
M	45	165	61.88	94	5
N	45	175	65.63	93	5
W	45	170	63.75	95	5
X	45	165	61.88	96	5

where *t* is the etching time in seconds and Δd is the thickness difference from before and after the etch.

The etch rate is reported to vary with time and temperature (Figures 4.2 and 4.3). The trend lines for each scatter plot match with a polynomial regression and not a linear line, which means there is nonlinear affiliation between the predictor variable x (time or temperature) and the expected value y (rate). The etch rate is the variable and is seen to increase as the wafer is submersed in the solution for a longer period of time. The corresponding regression equation for the etch rate by seconds is:

$$y = 0.0398x^2 - 0.4485x + 1.8519 \quad (5)$$

where *x* (s), is the predictor variable time and *y* (µm/min) is the corresponding etch rate.

Between the two quantities of rate and temperature the regression equation is:

$$y = 0.0108x^2 - 0.383x + 2.8676 \quad (6)$$

where *x* is the temperature and *y* is the corresponding etch rate.

Table 4.2 shows the average etch rate at the tested times as well as the standard deviation of the sample. The results show a better prediction of the etch rate at lower times due to the increasing standard deviation as the times increase. It is believed that the increase in standard deviation is caused by the inconsistent dilution of the etchant at the end of the etch process, as described in 3.2.2.

As the DI water is added to the etching container, the etching process will

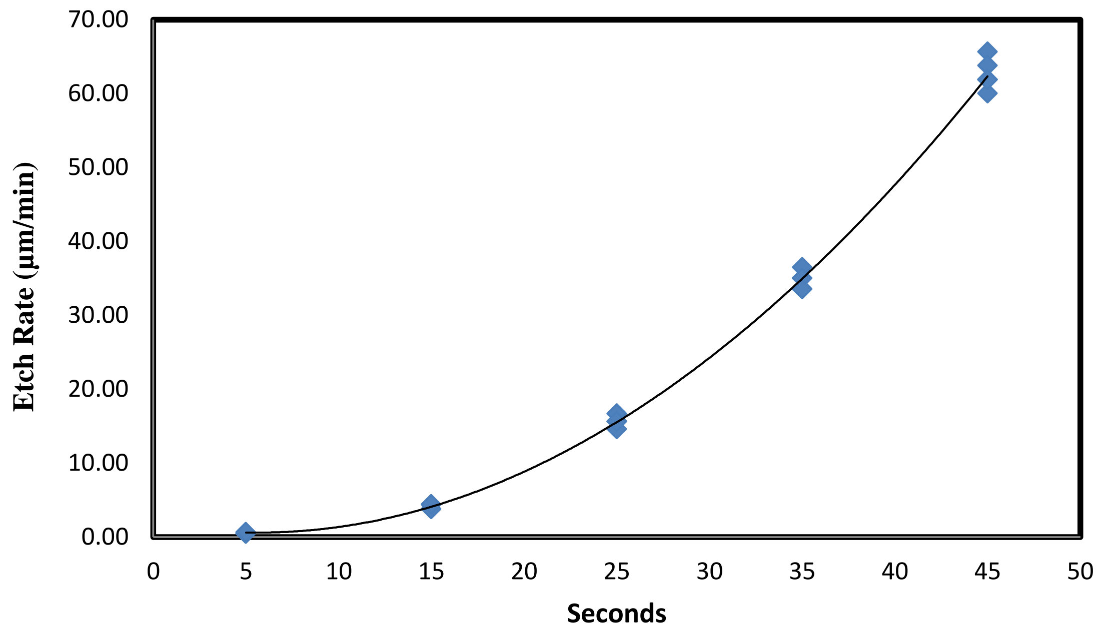

Figure 4.2 Etch rate of of $CuNO_3$ (10%) : HNO_3 : HF (1:1:2) solution on germanium wafer.

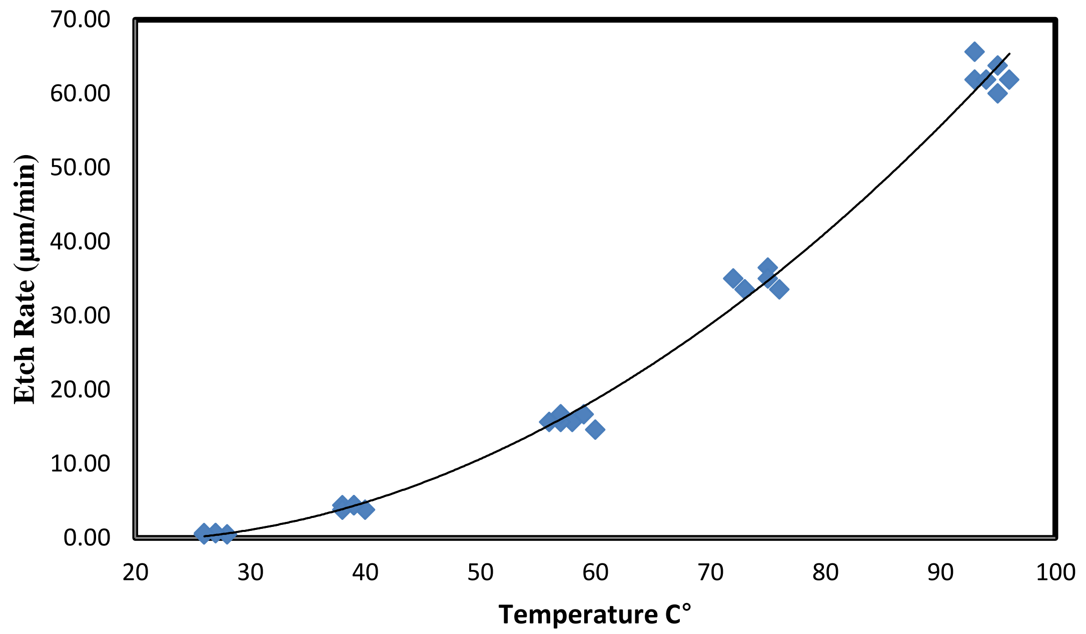

Figure 4.3 Etch rate of $CuNO_3$ (10%) : HNO_3 : HF (1:1:2) solution on germanium wafer as a function of etch temperature.

Table 4.2. Average etching rates for different times.

Etch Time (Sec)	**Mean Rate (µm/min)**	**Median Rate (µm/min)**	**Standard Deviation**	**Skewedness Value**
5	0.52	0.52	0.11	0
15	4.16	4.38	0.32	-0.97
25	15.79	15.63	0.78	-0.31
35	34.51	34.27	1.19	0.87
45	62.5	61.88	1.93	0.67

continue, especially between the bottom of the wafer and the container, and the complete dilution will vary between samples. With the measurement resolution on the order of microns some variation is expected.

The removal of material, for each etch time, is shown as a scatter plot in Figure 4.4. Comparing these data along with the data in Table 4.2, some statistics of each etching time can be inferred. When looking at the resulting etch rates, for 15 and 25 seconds, the distribution is slightly skewed to the left due to the mean being less than the median, and 35and 45 seconds have distributions that are marginally skewed to the right, means that are greater than the median. Overall each of the five etching times have small skewness and standard deviation values and a use of the mean etch rate, and corresponding time and temperatures would provide fairly accurate results.

Utilizing the polishing process reported here, the etch times of 35-45 seconds was ideal in decorating dislocation etch pits and low angle grain boundaries without over etching the wafer, which might mask dislocation etch pits. Figures 4.4-4.9 show etch results from each of the times tested. Markings that appear to be etch pits begin to be visible after 15 seconds and become distinct between 35 and 45 seconds. Though pits were seen after 25 seconds, as seen in Table 4.1, fully developed pyramidal shapes were not perceived until after that time, and fully developed pyramidal shapes were not consistent until after 45 seconds. Because of the need to quickly scan the wafer for dislocations etch pits, and the low desired etch pit density ($<200/cm^2$), the 45 seconds of etch time became the standard due to the large, but not over etched, pits seen after that time.

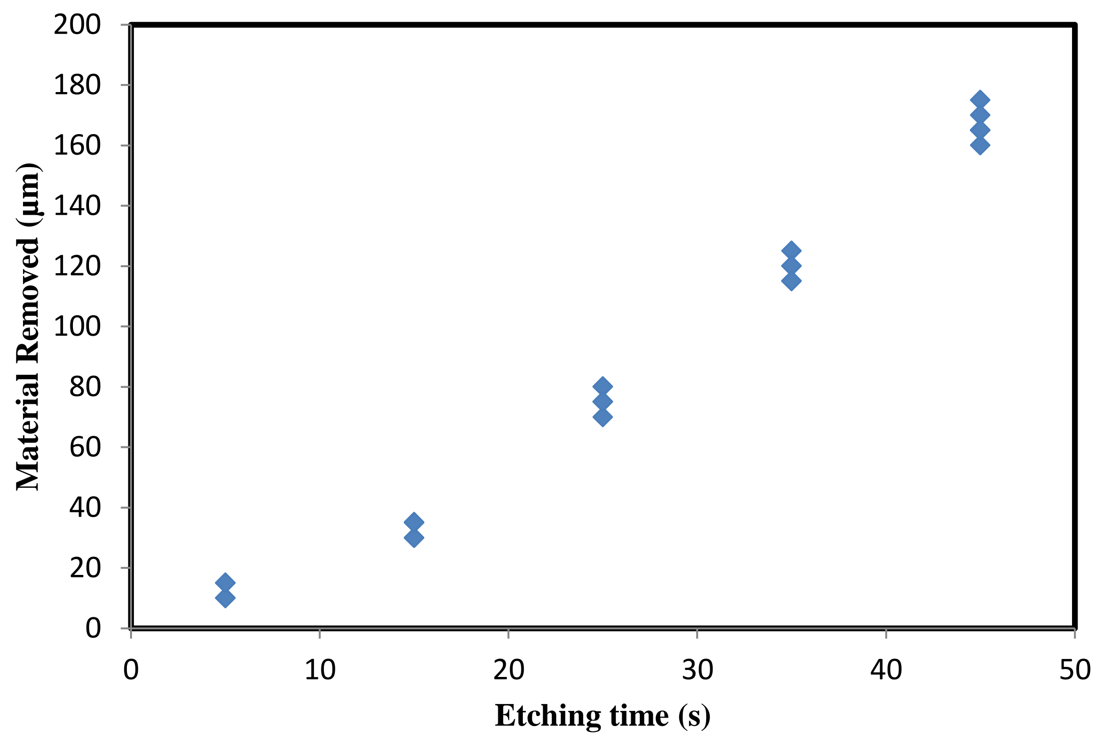

Figure 4.4 Removal of material at each etching time tested.

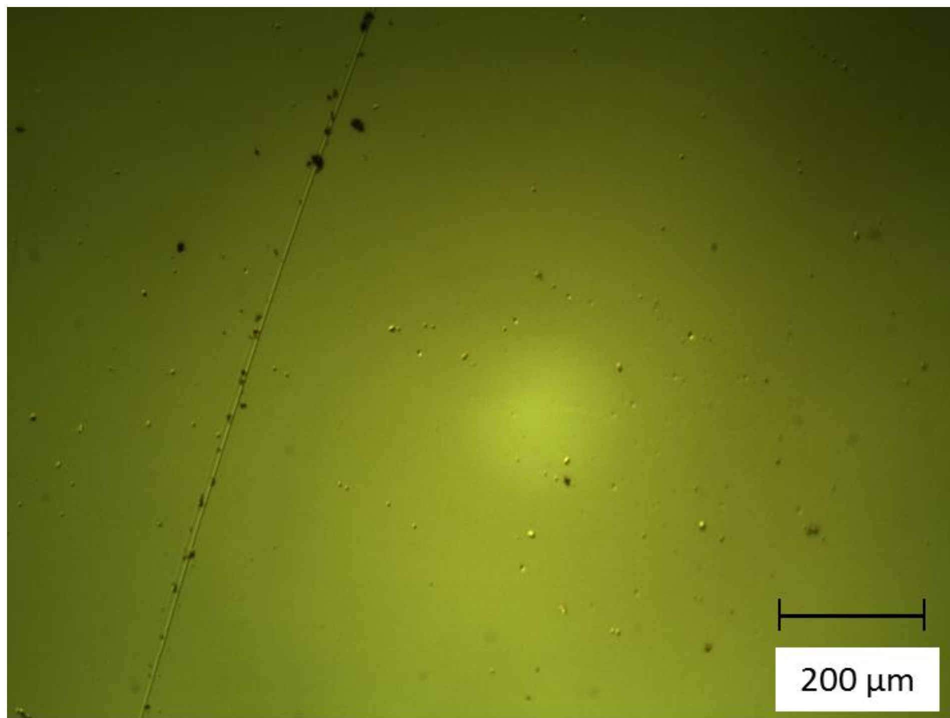

Figure 4.5 Image of germanium wafer surface after 5 seconds of etching using $CuNO_3$ (10%) : HNO_3 : HF (1:1:2) solution.

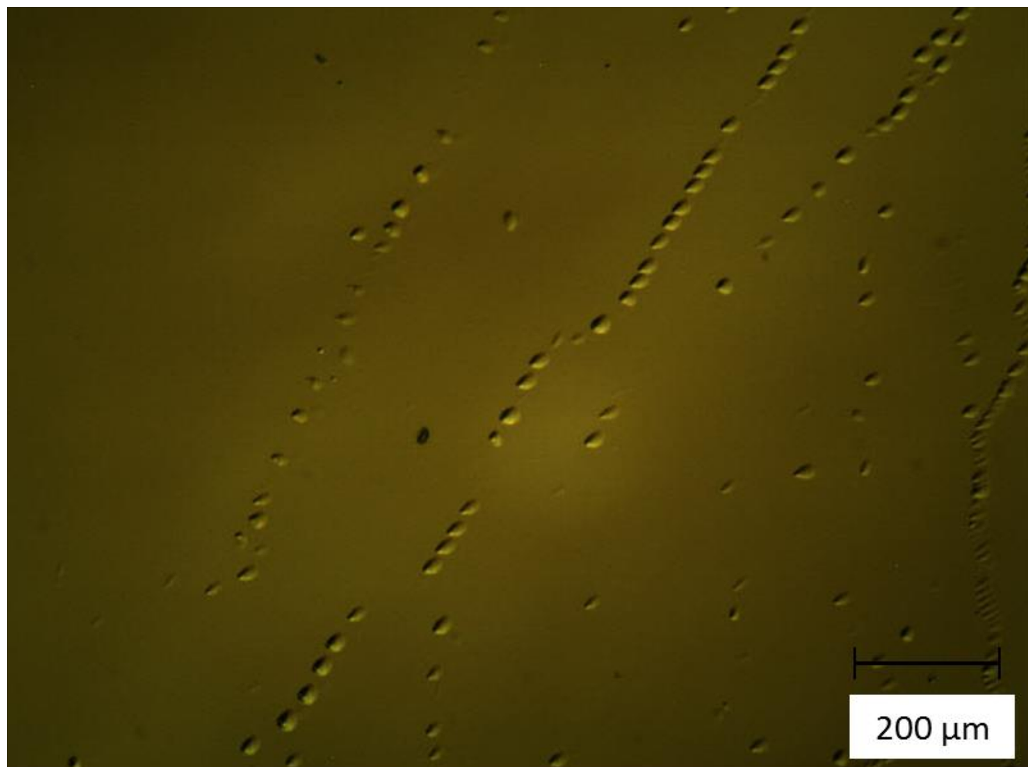

Figure 4.6 Image of germanium wafer surface after 15 seconds of etching using $CuNO_3$ (10%) : HNO_3 : HF (1:1:2) solution.

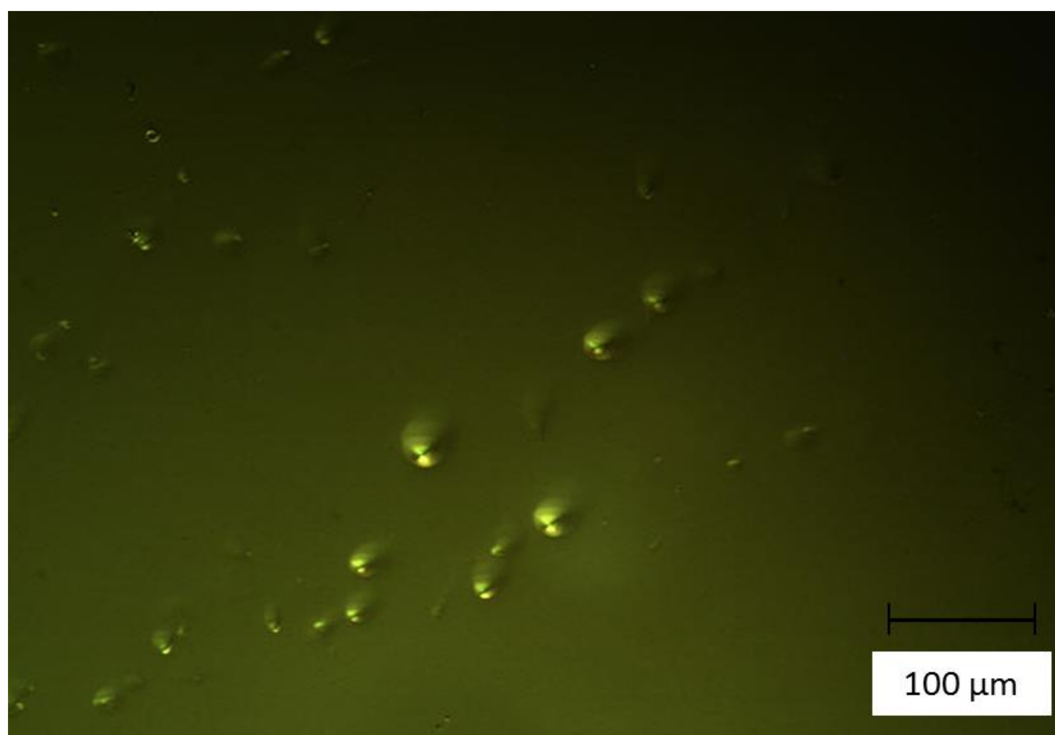

Figure 4.7 Image of germanium wafer surface after 25 seconds of etching using $CuNO_3$ (10%) : HNO_3 : HF (1:1:2) solution.

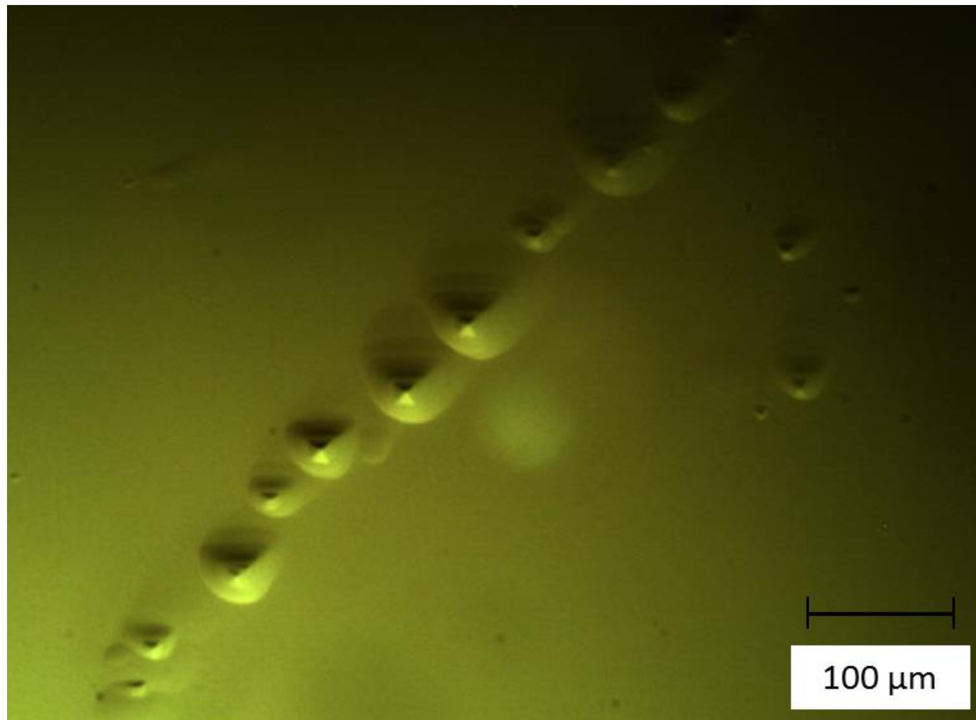

Figure 4.8 Image of germanium wafer surface after 35 seconds of etching using $CuNO_3$ (10%) : HNO_3 : HF (1:1:2) solution.

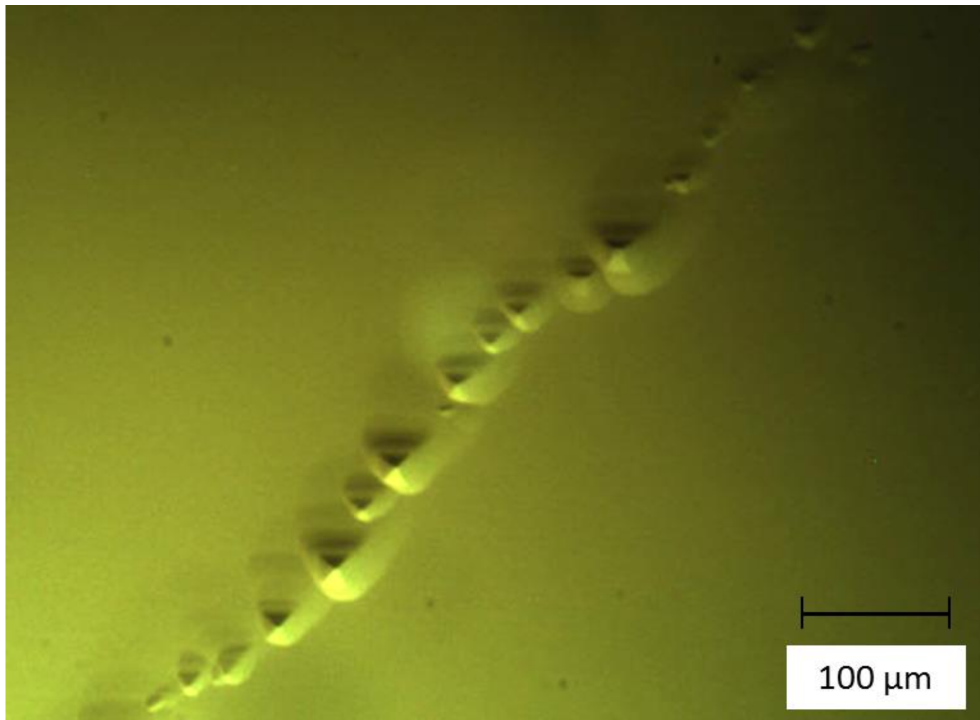

Figure 4.9 Image of germanium wafer surface after 45 seconds of etching using $CuNO_3$ (10%) : HNO_3 : HF (1:1:2) solution.

4.3 Alternative Polishing and Etching Processes

In the experimental techniques reported by Haller's study the samples were polished by a different technique than is reported here. Their germanium samples were "first lapped with 600 and 1900 grit lapping compound and then polish-etched in a 7:2:1 mixture of HNO_3, HF and red fuming HNO_3" [27].

After the etching solution and times were optimized, an experiment was done to find a chemical polishing process, to reduce the time needed to polish each test wafer and still provide the surface needed for preferential etch and decoration of dislocations.

After an additional 4 months of trials, with etchants that were known to etch the surface of these wafers but not decorate dislocations (Table 3.2) a process was developed. Wafers were cut from the crystal using either an ID saw or single wire saw, that sat in a bath of Hydrochloric Acid (HCl) for 5 minutes, to remove an oxide layer of the germanium, which were then polished etched using an initial step of 3:1 solution of HNO_3:HF and then a 1:1 solution of H_2O_2:HF. It is reported that these wafers had a polished surface sufficient for preferential etch. Dislocation etch pits and low angle grain boundaries were consistently revealed after being polished using this method and etched using the $CuNO_3$ (10%) : HNO_3 : HF solution.

In addition to the development of the polish etch, the data generated during this study also led to the reduction in etching times needed to reveal fully developed pits, as described in Section 4.2. After the blind tests, it was understood that the etching rate not only increased as the time of submersion increased but also as the temperature increased (Figures 4.2 and 4.3). Studying these graphs, along with the data in Table 4.1, it is understood that only until the etch rate is increased, and enough material is

removed from the surface, that pits are seen. After this supplementary study we began utilizing a warm etch, where the solution was preheated to a temperature of 60° C, which changed the initial etch rate to just under 20µm/min from the previous 0 µm/min. With the change in temperature the etch time was reduced to 30 seconds in order to see fully developed pits.

In addition to the wafers cut from the grown crystal, germanium wafers that have been processed for manufacturing and polished on a double side polisher, using a chemical mechanical polish, have also been etched using the solution studied with successful results. Due to the minimal thickness of these wafers, <200 µm, the etch time was reduced to 35 seconds.

CHAPTER 5

CONCLUSION

An etching solution for p-type single crystal germanium oriented off the [100] plane, 4°-8° towards the [111] plane, was tested and found to preferentially etch and decorate dislocations. With its vital use in IR optics, gamma-radiation detectors, and lately, concentrator multijuction celestial and terrestrial based solar cells, the ability to locate these dislocations is paramount in developing a growth and wafering process for ultra thin germanium wafers.

Process conditions for the solution, originally published by Haller et al., consisting of $CuNO_3$ (10%) :H_2O_2:HF (1:1:2) have been optimized to give consistent and reliable dislocation etch pits and low angle grain boundaries on a cross section of germanium that meets the conditions above. Though the solution was found in literature for undoped germanium, this study was set up for p-Type, gallium-doped germanium with results that outline the etching rates and optimal times needed for material with conditions mentioned above. All this is done without any etching artifacts due to subsurface damage which might mask dislocation etch pits.

With no other published etching solution for germanium grown a few degrees off the <100> face, this study made it feasible to assess any growth process changes with a view to improving crystal perfection and increasing throughput in a production

environment. With the data gathered in this study, common etchants for germanium and also correlations between etching rates and etch times/temperatures, supplemental studies made it possible to remove the mechanical polishing step and replace it with an etch polish. A process of a warm etch was also developed, utilizing these data, which also reduced the etching times.

APPENDIX: VISUAL SCORE TABLE

Table A.1. Visual Score and description used for blinded study.

Score	Description
1	No pits seen
2	Small pits, no defined facets
3	Small pits, weak definition of facets
4	Larger pits, pyramid shape developing
5	Fully developed pits with pyramid shape defined

REFERENCES

1. C. Winkler, "Discovery of Germanium," (in German), *Berichte der Deutschen Chemischen Gesellschaft*, vol. 19, pp. 210-211, 1886.

2. S.M. Sze, *Physics of Semiconductor Devices*, 1st ed. New York: Wiley, 1969, pp. 22.

3. P. Clauws and E. Simoen,"Metals in Germanium," *E-MRS 2006 Spring Meeting*, Nice, FR., 2006, pp. 546-553.

4. S. Adachi, "Germanium," in *Handbook on Physical Properties of Semiconductors, Vol. 1*. Norwell: Kluwer Acad., 2004.

5. (7 Oct. 2010), *Spire Pushes Solar Cell Record to 42.3%* [Online], Available: http://optics.org/news/1/5/5.

6. R.K. Willardson and A.C. Beer, "Indium Phosphide: Crystal Growth and Characterization," *Semiconductors and Semimet*als, vol. 31, San Diego, Acad. Press, 1990

7. P.J Holmes, "Etch Pits on Dendritic Germanium. A Clarification," *Phys. Rev.,* vol. 119, no. 1, pp. 131-132, Jul. 1960

8. M.F. Ehman, et. al, "Morphology of Etch Pits on Germanium Studied by Optical and Scanning Electron Microscope," *J. Appl. Phy.*, vol. 41, no. 7, (1970) pp. 2824 – 2827, Jan. 1970.

9. T. Arizumi, and I. Akasaki, "Etch Patterns and Dislocation Etch Pits on Germanium with KI-I2 Redox System," *Jap. J. of Appl. Phys.*, vol. 1, no. 6, pp. 350, Dec. 1962.

10. B.W. Batterman, "Hillocks, Pits, and Etch Rate in Germanium Crystals," *J. Appl. Phys.*, vol. 28, no. 11, pp. 1236-1242, Jun. 1957.

11. A. Pajaczkowska (1998), *Professor Dr. Jan Czochralski-An Inventor* [Online], Available: http://www.ptwk.org.pl/pol/documents/dgkk73.pdf

12. G.K. Teal and J.B. Little, "Growth of Germanium Single Crystals," *Phys. Rev.*, vol. 78, no. 5, pp. 647, 1950.

13. P. Spiewak, et al., "Simulation of Intrinsic Point Defect Properties and Vacancy Clustering During Czochralski Germanium Crystal Growth," *Mat. Sci. in Semiconductor Processing,* vol. 9, pp. 465-470, Sep. 2006.

14. S. Franssila, *Introduction to Microfabrication,* 2nd ed., Chester, U.K.: Wiley, 2010, pp. 36-60.

15. G. Müller, "*Fundamentals of Melt Growth,"* 13th Int. Summer School on Crystal Growth, Park City, UT, 2007, pp. 13.

16. R.N. Hall, "Segregation of Impurities During the Growth of Germanium and Silicon Crystals," *J. Of Phy. Chem*., vol. 57, pp. 836-839, 1953.

17. Kodera, H., 1963, "Constitutional Supercooling during the Crystal Growth of Germanium and Silicon," *Jap. J. Of Applied Phys.*, vol. 2, no. 9, pp. 528, 1963.

18. D. T. J. Hurle, *Crystal Pulling from the Melt*, Springer, Berlin, Ger. 1993.

19. E. Billing, "Some Defects in Crystal Growth from the Melt I. Defects caused by Thermal Stress," *Proc. of the Royal Soc. of London. Series A, Math. and Phy. Sci.*, vol. 235, no. 1200, pp. 37-55, 1955.

20. R.S. Wagner, "Production of Dislocations in Germanium by Thermal Shock," *J. Appl. Phys*., vol. 29, no. 12, pp. 1679-1682, 1958.

21. I. Yonenaga and K. Sumino, "Mechanical Strength of GeSi alloy," *J. Appl. Phys*., vol. 80, no. 6, pp. 3244-3247, 1996.

22. Cor Claeys and Eddy Simoen, eds. *Germanium-Based Technologies From Materials to Devices,* Oxford, UK: Elsevier, 2007.

23. P. Blau, "Surface Damage," in *Friction*, *lubrication and Wear Technologies,* 18th ed. Metals Park: ASM, 1992.

24. A. Haapalinna, S. Nevas, and D. Pahler, "Rotational Grinding of Silicon Wafers Sub-surface Damage Inspection," *Mat. Science and Eng. B*, vol. 107, pp. 321-331, 2004.

25. F.L. Vogel et al., "Observations of Dislocations in Lineage Boundaries in Germanium," *Phys. Rev*. vol. 90, no. 3, pp. 489-490, 1953.

26. S. Wang, et al., "The Evaluation and Modeling of the Chemical Mechanical Planarization (CMP) Removal Rate for Polysilicon," *NanoTech* 2004.

27. G. Hubbard and E. Haller, "Electrical Properties of Dislocations in Ultra-Pure Germanium," *21st Electronic Conf.*, Boulder, CO., 1979.

28. M. F. Ehman, et al., "Morphology of Etch Pits on Germanium Studies by Optical and Scanning Electron Microscopy," *J. of Applied Physics*, vol. 41, no.7, pp. 2824-2827, 1970.